Late Pleistocene–Holocene (52–10 ka) microstratigraphy, fossil taphonomy and depositional environments from Tam Pà Ling cave (northeastern Laos)

F Demeter, V C Hernandez, M W Morley, A-M Bacon, P Duringer, K E Westaway, R Joannes-Boyau, J-L Ponche, C Zanolli, P Sichanthongtip, et al.

▶ **To cite this version:**

F Demeter, V C Hernandez, M W Morley, A-M Bacon, P Duringer, et al.. Late Pleistocene–Holocene (52–10 ka) microstratigraphy, fossil taphonomy and depositional environments from Tam Pà Ling cave (northeastern Laos). Quaternary Science Reviews, 2024, pp.108982. 10.1016/j.quascirev.2024.108982 . hal-04745808

HAL Id: hal-04745808
https://hal.science/hal-04745808v1

Submitted on 21 Oct 2024

HAL is a multi-disciplinary open access archive for the deposit and dissemination of scientific research documents, whether they are published or not. The documents may come from teaching and research institutions in France or abroad, or from public or private research centers.

L'archive ouverte pluridisciplinaire **HAL**, est destinée au dépôt et à la diffusion de documents scientifiques de niveau recherche, publiés ou non, émanant des établissements d'enseignement et de recherche français ou étrangers, des laboratoires publics ou privés.

Distributed under a Creative Commons Attribution - NonCommercial - NoDerivatives 4.0 International License

Quaternary Science Reviews xxx (xxxx) xxx

Contents lists available at ScienceDirect

Quaternary Science Reviews

journal homepage: www.elsevier.com/locate/quascirev

Late Pleistocene–Holocene (52–10 ka) microstratigraphy, fossil taphonomy and depositional environments from Tam Pà Ling cave (northeastern Laos)

V.C. Hernandez [a,*], M.W. Morley [a], A.-M. Bacon [b], P. Duringer [c], K.E. Westaway [d], R. Joannes-Boyau [e], J.-L. Ponche [f], C. Zanolli [g], P. Sichanthongtip [h], S. Boualaphane [h], T. Luangkhoth [h], J.-J. Hublin [i,j], F. Demeter [k,l]

[a] Flinders Microarchaeology Laboratory, College of Humanities, Arts and Social Sciences, Flinders University, South Australia, Australia
[b] Université Paris Cité, CNRS, BABEL, UMR, 8045, 75012, Paris, France
[c] Ecole et Observatoire des Sciences de La Terre, Institut de Physique du Globe de Strasbourg (IPGS), UMR, 7516, CRNS, Université de Strasbourg, Strasbourg, France
[d] School of Natural Sciences, Faculty of Science and Engineering, Macquarie University, Sydney, Australia
[e] Geoarchaeology and Archaeology Research Group (GARG), Southern Cross University, Lismore, NSW, Australia
[f] Université de Strasbourg, Laboratoire Image, Ville Environnement, UMR, 7362, UdS CNRS, Strasbourg, France
[g] Univ. Bourdeaux, CNRS, MCC, PACEA, UMR 5199, F-33600, Pessac, France
[h] Ministry of Information, Culture and Tourism, Vientiane, PDR, Laos
[i] Chaire de Paléoanthropologie, CIRB (UMR 7214-U1050), Collège de France, 11 Place Marcelin-Berthelot, 75231, Paris, Cedex 05, France
[j] Max Planck Institute for Evolutionary Anthropology, Deutscher Platz 6, Leipzig, Germany
[k] Lundbeck Foundation GeoGenetics Centre, Globe Institute, University of Copenhagen, Copenhagen, Denmark
[l] Eco-anthropologie (EA), Dpt ABBA, Muséum National d'Histoire Naturelle, CNRS, Université Paris Cité, Musée de L'Homme, Paris, France

ARTICLE INFO

Handling editor: Donatella Magri

Keywords:
Pleistocene
Holocene
Homo sapiens
Southeast Asia
Micromorphology

ABSTRACT

Fossil evidence for some of the earliest *Homo sapiens* presence in mainland Southeast Asia have been recovered from Tam Pà Ling (TPL) cave, northeastern Laos. Taphonomic indicators suggest that these human fossils washed into TPL via gradual colluviation at varying times between MIS 5–3, yet no attempt has been made to situate them within the depositional environments of the cave within these periods. This has precluded a deeper appreciation of their presence there and in the surrounding landscape. In this first microstratigraphic study of TPL, we primarily use sediment micromorphology to reconstruct the depositional environments of the cave, relate these environments with the taphonomic history of the human fossils recovered from the upper 4 m of the excavated sequence, and explore how the sediments can better explain the presence of these humans in the area during MIS 3–1 (52–10 ka). Our results demonstrate changes in local ambient conditions from being temperate to arid, with ground conditions often wet during MIS 3 and becoming increasingly seasonal (wet-dry) during MIS 2–1. The changing cave conditions impacted its interior topography and influenced the way sediments (and fossils) were deposited. Preserved combustion biproducts identified in the sediments suggest two possible scenarios, one where small forest fires may have occurred during periods of regional aridity and/or another where humans visited the cave.

1. Introduction

The excavations in Tam Pà Ling (Cave of Monkeys), northeastern Laos (Fig. 1A), have unearthed a fossil assemblage of *Homo sapiens* that is unique for the study of Late Pleistocene human evolution in Southeast Asia (SEA) (Demeter et al., 2012; Demeter et al., 2015; Demeter et al., 2017; Shackelford et al., 2018; Freidline et al., 2023). The fossil assemblage is formed of a partial cranium (*TPL1*), two mandibles (*TPL2*, *TPL3*), a partial rib (*TPL4*), a proximal pedal phalanx (*TPL5*), a partial frontal (*TPL6*), and a tibial fragment (*TPL7*), all excavated from a trench situated deep inside the cave. Although disarticulated, the fossils otherwise display minimal evidence of remobilisation or physical abrasion, a rare occurrence from the region (Lee and Hudock, 2021; Sawafuji et al., 2024). As such, the fossils have helped demonstrate the major morphological variations that existed between the different populations of *Homo sapiens* in SEA during the Late Pleistocene (Demeter

* Corresponding author.
E-mail address: vito.hernandez@flinders.edu.au (V.C. Hernandez).

https://doi.org/10.1016/j.quascirev.2024.108982
Received 6 August 2024; Received in revised form 18 September 2024; Accepted 20 September 2024
0277-3791/© 2024 The Authors. Published by Elsevier Ltd. This is an open access article under the CC BY-NC-ND license (http://creativecommons.org/licenses/by-nc-nd/4.0/).

Fig. 1. (**A**) Location of Tam Pà Ling (20°12′33.41"N, 103°24′22.02"E). Red square indicates the study area. (**B**) Pà Hang hill with Tam Pà Ling and other studied sites labelled (Photograph: P. Duringer) (**C**) Access to T3 (lit area) (Photograph: V.C. Hernandez). (**D**) Plan of Tam Pà Ling (Redrawn after J.-L. Ponche and P. Duringer). (**E**) Studied section showing locations of micromorphological sampling and levels where *TPL1*, *2*, and *5* were recovered (dashed orange line) (Photograph V. C. Hernandez).

et al., 2017), consequently making Tam Pà Ling (TPL) a key site for the study of the evolution and dispersal of our species in the Far East (Matsumura et al., 2019; Demeter and Bae, 2020; Hublin, 2021; McAllister et al., 2022; Sawafuji et al., 2024).

The TPL fossils represent some of the earliest evidence for *Homo sapiens* in continental SEA, deposited in the cave at different times between Marine Isotope Stage (MIS) 5b and MIS 3 (~87–30 ka) (Freidline et al., 2023). Although some of the fossils have been directly dated via uranium–thorium methods, their dates are reported only as minimum age estimates (Demeter et al., 2012, 2015). This is largely due to the unaccounted profiles of uranium from the sampled deposits, noting that tropical environments hold the potential of enhancing heterogeneous distribution of uranium in bones that are chemically weathered in situ. Hence, the modelled depositional ages (2σ) of the containing sediment matrix are preferred when referring to the age of the fossils, with the oldest returned age estimate being ~86 ka, supporting a much earlier dispersal of *Homo sapiens* into SEA than previously known. Details of the modelled depositional chronology of TPL are published in Freidline et al. (2023).

Whereas palaeoenvironmental reconstructions of the landscape surrounding TPL have provided some context to understand the early dispersal of *Homo sapiens* in SEA (Milano et al., 2018; Bourgon et al., 2021; McAllister-Hayward et al., 2024), there is still very little understanding of their presence at the site and in the local catchment, other than the occurrence of the fossils. This largely precludes the development of more detailed scenarios for the early *Homo sapiens* settlement of Asia (Dennell, 2017) and achieving a better understanding of their adaptations to environmental changes in tropical landscapes, which are argued to play an important role in human evolution and dispersals in the deep past (Scerri et al., 2022 and references therein). In SEA, such knowledge remains elusive due to the limited evidence from the Pleistocene archaeological record and the current resolution of ages that frame the presence of humans at many of the studied sites.

While the ages of the fossils from TPL are well-constrained, the absence of artefacts or occupation surfaces found to date suggests that humans did not intensively occupy the cave during the Late Pleistocene. However, evidence of human presence and occupation at neighbouring sites spanning the Middle Pleistocene to Late Holocene (Demeter et al., 2009; Patole-Edoumba, 2015; Bacon et al., 2021; Demeter et al., 2022, Fig. 1B), and the presence of the fossils from TPL, suggest that humans may have at least visited sporadically or used the cave in the past, even briefly. If so, then traces of their activities from the entrance or even inside might still be preserved, although likely in small quantities, probably degraded, diagenetically altered, or buried beneath limestone slabs.

The research at TPL has simultaneously highlighted the scientific challenges of understanding archaeological site formation processes in the hot and humid tropics (Morley and Goldberg, 2017 and references therein), and the need to better understand geomorphological processes that affect the interpretation and dating of fossils from cave sites (Liu et al., 2015; Westaway et al., 2017; Yao et al., 2020). These challenges are made more difficult by the erratic preservation of organic materials in tropical cave environments (Louys et al., 2017 and references therein; Smith et al., 2020 and references therein), and therefore demand the systematic evaluation of the stratigraphy of a site with the potential to yield bioarchaeological data (e.g., aDNA, proteins) that can inform about humans and their environments in the past (Massilani et al., 2022; Morley et al., 2023; Aldeias and Stahlschmidt, 2024). It is for these reasons that there is a need to better understand the stratigraphy of TPL at various spatial scales (vertical and horizontal) and at finer resolution, with research from other sites in SEA suggesting a geoarchaeology-focused approach to achieve this (O'Connor et al., 2010; Morley, 2017).

Sediment micromorphology (microstratigraphy) is one method employed in geoarchaeological research that can help to better understand the geomorphological and site formation processes governing TPL. Research employing this method to study the critical sites for understanding early human evolution and dispersals in SEA show that microstratigraphy can provide a more nuanced picture of local environments in the past, help to reveal more about human adaptations to the different environmental conditions that existed, and temporally resolve the presence of humans on-site and in the immediate catchment (Stephens et al., 2005, 2017; Lewis, 2007; Brasseur et al., 2015; Mijares, 2017; Morley et al., 2017; McAdams et al., 2020; Anderson et al., 2024; Shipton et al., 2024). With these in mind, a program of microstratigraphic analysis at TPL was initiated to gain further insights into the history of the site and the taphonomy of the *Homo sapiens* fossils recovered from there.

To improve the understanding of the history of the site and taphonomy of *Homo sapiens* fossils recovered from TPL we link the results of the microstratigraphic analysis with loss-on-ignition (LOI) and magnetic susceptibility (χ) analysis of sediments. Both methods provide quick to obtain and accurate determinations of geochemical characteristics that can complement the interpretation of the microstratigraphic record (Stoops, 1978; Macphail and Goldberg, 2017). LOI, for instance, has complemented microstratigraphic analysis of archaeological cave sites in Malaysia, northern Vietnam and Thailand, resulting in a clearer understanding of the depositional environments that existed in these caves in the past (Hunt et al., 2007; Stephens et al., 2016; McAdams et al., 2020; Saminpanya and Denkitkul, 2020). While χ has been used at TPL to infer moisture availability that helped to reconstruct the vegetation surrounding the cave during the Late Pleistocene (Milano et al., 2018) and allowed insights into the timing of sediment delivery into the cave during periods of strengthened monsoons (Freidline et al., 2023). By linking the results of these analyses with that of the microstratigraphy, it is hoped that a clearer understanding of site formation and better explanation of the presence of humans at TPL is achieved.

Here, we present the results of the program to analyse the microstratigraphy, LOI and χ of sediments in TPL. Our geoarchaeological work aims to prove the efficacy of a microstratigraphic approach to understanding the important stratigraphy of the site by reconstructing its ground conditions, clarifying the taphonomic history of the fossils related to the depositional history of the cave, and exploring the potential archaeology within its sediments. By doing so, we try to resolve how past conditions in TPL (sediment, cave, and catchment) affect the interpretation of human presence at the site and explore how this information changes the narrative of Late Pleistocene human evolution and dispersals in the Far East. We focus the analyses on the upper 4 m Late Pleistocene–Holocene sediment sequence exposed in the 7 m-deep excavation inside the cave. This upper sequence was securely dated to between 46 ± 6 ka and 13 ± 3 ka (Freidline et al., 2023) and was where the human fossils *TPL1*, *2* and *5* were recovered (Demeter et al., 2012, 2015, 2017).

2. Tam Pà Ling: regional context and palaeoenvironmental setting

TPL is a limestone cave that has a large and relatively flat sediment-filled chamber that measures ~30 m in length, ~40 m in width, and ~12 m in height. Access to the chamber is via a steep (~30°), ~69 m-long talus slope, covered by large limestone slabs and blocks (up to ~5m in size) from a south-facing opening covered by forest vegetation (Fig. 1C). Three trenches have been excavated in the chamber. The largest trench, Trench 3 (T3), where the human fossils were recovered, is located at the eastern end (Fig. 1D; Freidline et al., 2023). A ~7 m sequence of sandy and silty clays, occasional limestone clasts, and intercalated fine calcareous precipitates formed on top of several massive limestone slabs is currently exposed in T3. Together with the occasional limestone clasts, clays, primarily vermiculite and kaolinite, quartz and secondary oxides are allogenic and appear to derive from the entrance of the cave via slow colluvial processes. (Demeter et al., 2012, 2015; Shackelford et al., 2018; Freidline et al., 2023). In T3, these

processes form discrete and undisturbed layers primarily substantiated by unobservable bioturbation and soft deformation on the exposed sections (Fig. 1E).

TPL is located ~1170 m above sea level at the top of the Pà Hang hill in the northern end of the Annamite Mountain range (AMR) (Fig. 1B), which is primarily a karstic environment of Upper Carboniferous–Permian sinkholes, towers, caves, and caverns (Duringer et al., 2012). This environment is formed by the vertical movement of faults dissecting a basement of diorite and granite capped by arkosic sandstones and limestones (Fromaget and Saurin, 1936; Saurin, 1969). Based on the present Köppen-Geiger classification, the northern end of the AMR lies within an intermediate zone of tropical savannah and temperate climates experiencing dry winters and hot summers (Beck et al., 2018). The temperatures here range ~18–35 °C, with extreme humidity from March to May caused by the Indian Ocean Monsoons and Subtropical High (Nguyen-Le et al., 2015) and heavy rainfall from June to August caused by the East Asian Monsoons (Chabangborn et al., 2014).

Several palaeoenvironmental studies demonstrate closed canopy forests (C_3 vegetation) to have covered TPL to varying extents from MIS 5–1, with the analyses on materials directly sampled from the site providing the most immediate picture of its surrounding landscape (Milano et al., 2018; Bourgon et al., 2021; McAllister-Hayward et al., 2024). These studies suggest that during MIS 3, when the *TPL2*, *5* and *1* human fossils were deposited, the moisture availability during the different stadials, interstadials and Heinrich events that characterised this stage would have led to varying gaps in the canopy cover (McAllister-Hayward et al., 2024). By MIS 2, beginning the LGM, the research indicates that a more open and mosaic landscape existed around TPL, which was likely distinguished by a mix of closed canopy forests (C_3 vegetation) and grasslands (C_4 vegetation). Finally, by MIS 1, the research implies a return to a more closed canopy forest landscape that is likely similar to what it is today.

3. Methods

3.1. Field observations and sampling

To better constrain the depositional environments at TPL from ~52 to 10 ka and the taphonomic history of its human fossils deposited between ~52 and 30 ka, we conducted sediment logging and sampling of the upper 4 m of the excavated sequence. The compaction, structure (if any), colour, texture of sediments, and boundary between units (where visible) were recorded (Supplementary Table 1). The sampled area was positioned immediately adjacent to the human fossil findspots (Fig. 1D). Four intact sediment blocks were collected for microstratigraphic analysis. The blocks were taken from levels that stratigraphically associate with the *TPL1*, *2*, and *5* fossils and from levels where distinct changes in the stratigraphy were noticed (Fig. 1E). These blocks measured ~20 cm high, 10 cm wide, and 10 cm thick. Gypsum plaster bandages were used to stabilise them for transit to the Flinders Microarchaeology Laboratory in South Australia. To complement the microstratigraphic analysis, eighteen disaggregated sediment samples were collected for LOI and χ analysis at the same laboratory. These sediment samples were collected next to where the block samples were retrieved in a column from ~3.7 to 0.2m below the excavation surface (Supplementary Table 1).

3.2. Sample preparation and analysis

3.2.1. Microstratigraphy

Microstratigraphy employs a variety of imaging techniques and microscopes (i.e., polarising, scanning electron) to describe the physicochemical properties of sediments and analyse them in their unique microstratigraphic contexts (microfacies) preserved in thin sections (Courty, 2001; Weiner, 2010; Macphail and Goldberg, 2017; Stoops, 2018). The method permits the detailed (microscale) reconstruction of the depositional (e.g., stream deposition) and post-depositional (e.g., carbonate precipitation) processes that formed a site, and possibly the identification of features that associate with human activity such as trampling, building of hearths, and sweeping (Goldberg and Aldeias, 2018). The collected block samples were oven dried at 35 °C for ~7–8 days and prepared for thin section production using a mixture of clear polyester casting resin, monomer styrene, and methyl ethyl ketone peroxide (MEKP) following procedures outlined by Morley et al. (2017). When fully cured, these hardened blocks were cut into smaller, wafer-size portions and sent to the Adelaide Petrographics Ltd laboratory for the manufacture of 30 μm-thick thin sections (75 × 45 mm).

Thin sections were scanned on a flatbed scanner, once with the lid closed to simulate a transmitted light image, and once with the lid open to simulate a dark light image. The latter delimits highly reflective Fe- and calcite-rich features in thin sections (Goldberg and Aldeias, 2018). A Leica DM 2700 P (polarising) microscope fitted with a Leica MC 1900 HD camera was used to capture images in thin section from 25 to 400× magnification under plane-polarised (PPL) and cross-polarised (XPL) light. A ThermoFisher Phenom XL benchtop scanning electron microscope with an energy dispersive spectroscope (SEM/EDS) was used to identify and map elements within regions of interest in the thin sections between 600 and 2050× magnification. The observed features were described following guidelines outlined in Stoops (2021).

3.2.2. Magnetic susceptibility

The results of χ analysis are often used as climatic indicators, where elevated χ values correspond to intermittent periods of wetting and drying (increased seasonality), and dry or excessively wet and acidic sediments correspond to lower χ values (Evans and Heller, 2003). Because soil formation and burning, possibly as a result of human activity, have the tendency to enhance the magnetic qualities of sediments, χ values are also used to interpret these phenomenon (Tite and Mullins; Lowe et al., 2016). However, research employing this method on archaeological sites show that to accurately interpret local climate conditions and assess the contribution of anthropogenic sediments to the sedimentary record results need to be contextualised in well-known and dated stratigraphic sequences (Kehl et al., 2014; Bradák et al., 2020; Dinckal et al., 2022).

To analyse for χ, disaggregated sediment samples were oven-dried at 40 °C for ~7–8 days. The dried samples were ground to achieve a fine and consistent grain-size (<125 μm). ~29–31 g aliquots were subsampled, and, following the protocols set by Dearing (1994), a Bartington MS2 magnetic susceptibility indicator accounted for the low (470 Hz) and high frequency (4.7 kHz) χ of each sample in standard international units (10^{-6} m^3/kg). Here, only the low-frequency magnetic susceptibility of sediments (χ_{LF}) is reported since it is the most sensitive to magnetic changes (Lowe et al., 2016).

3.2.3. Loss-on-Ignition

LOI analysis provides estimates of organic matter (OM) and carbonate content (CC) in sediments by measuring the weight loss of dry bulk density of sediment after ignition at different temperatures (Heiri et al., 2001). In research conducted in caves, LOI has been used mostly to distinguish sediment provenance and account for post depositional carbonate precipitation, helping to reconstruct the history of a site alongside other sedimentological and geochemical methods of analysis (Piló et al., 2005; Skaberne et al., 2015a; Skaberne et al., 2015b; Benedetti et al., 2019)

To determine OM and CC, the same sediment samples analysed for χ were utilised. Following the LOI protocol of Heiri et al. (2001), a time-programmed Across International CF 1200 series muffle furnace with 36-L chamber capacity incinerated samples. The following equations were used to calculate the percentage of OM and CC in each sample, where DW_x refers to the dry weight of samples and temperature at which they were incinerated.

For OM: $LOI_{550}=((DW_{105} - DW_{550})/DW_{105})*100$

For CC: $LOI_{950}=((DW_{550} - DW_{950})/DW_{105})*100$

4. Results

4.1. Stratigraphy and micromorphology

The upper 4 m of the TPL stratigraphy can be divided into ten lithological units comprised mostly of silts and clays. Nine of these units were fully observed in the exposed section and described (Supplementary Table 1). Boulder and cobble-sized rockfall from cave attrition are distributed towards the base (Unit 10 and 9) and occur in Units 8,3 and 1 (Fig. 2). Units 8–5 are of interest. They comprise sediments from where the human fossils *TPL1*, *2*, and *5* were recovered, and layers that date to the Late Pleistocene–Holocene ~52–10 ka (Freidline et al., 2023, Fig. 2). Limestone spalls from cave attrition are distributed in Unit 9, and in Unit 8 from ~2.34 to 2.5 m. Throughout Unit 8, Mn nodules are ubiquitous, and gravel stringers are recurrent with occasional $CaCO_3$ inclusions often appearing as powdery nodules. Units 7–5 are characteristically $CaCO_3$- and silt-rich, with Unit 6 having more clay and gravels. The interface between Unit 5–4 is also reported here. Their boundary is sharp, marking the transition to the Holocene.

Ten thin sections were produced from the four sediment blocks (Fig. 2) sampled for microstratigraphic analysis. The thin sections were representative of the sedimentary variations in each block. Fifteen microfacies were identified from these thin sections. A summary of the micromorphological characteristics of these facies is presented in Table 1 and explained in subsections 4.1.1.–4.1.7 from the base up of the sequence.

4.1.1. Lower region of unit 8 (Thin section MM4C and MM4A)

The lower part of Unit 8, where the *TPL2* and *5* fossils come from, is formed of dark reddish-brown clays and calcareous silts deposited ~52–40 ka (Fig. 2, Supplementary Table 1). MM4C (Fig. 3A) and MM4A represent this region characterised by one microfacies, mf 8a. (Table 1). Here, limestone spalls are mostly subangular, with a few being severely etched (Fig. 3B), which likely reflects its long period of burial in damp clays and improbability of having been reworked from afar. Microcharcoal is well-preserved (Fig. 3C) and occur alongside amorphous nodules of micritic calcite, likely plant ash (Canti, 2003) preserved through phosphatisation (Karkanas, 2021).

Most of the gravel–sand-sized inclusions in mf 8a are moderately to well-sorted in horizontally lain sediment stringers, which grade into finer fractions (gravel to sands) up sequence. They are recurrent and form part of several (often carbonate-rich) microlaminations, better seen under dark field light (Fig. 3A). Neoformed sparite is rare but often developed in the planar voids, suggesting that these minerals are formed during the occasional drying of the sediments as sediment cracking is a feature of desiccation. Most of the spalls are Fe-stained or phosphatised (Fig. 3A), and along with the Mn-rich features in the sediment (stains and nodules) are indicative of a redoximorphic environment (Vepraskas et al., 2018). Apart from a few ash and Mn nodules ranging between ~5 and 10 mm Ø, a conglomerated clast composed of phosphatised calcite cemented on a clay clast form part of coarse-sized sediments in thin section MM4A (Fig. 3D). SEM-EDS analysis of the clay clast reveals a closed context of microcharcoal, ash and oxidised Fe-rich clays (Fig. 3D and E).

4.1.2. Upper region of unit 8 (Thin sections MM3B and MM3A)

The upper part of Unit 8 is comprised of limestone spalls, gravel clasts, and recurrent fine gravel and sand stringers intercalating reddish-brown silty clays (Fig. 2, Supplementary Table 1). MM3B and MM3A are representative of this region in the stratigraphy, and three microfacies (mf 8b–8d) are identified in these thin sections (Table 1).

Mf 8b is associated with sediments deposited ~48–30 ka and the *TPL1* human fossil (Fig. 2; Table 1). Mf 8b is less compact than mf 8a, having more void spaces, with prominent planar voids dipping ~30° downslope towards the cave wall (Fig. 4A). Most coarse inclusions follow the same downward dip as the voids. These inclusions comprise numerous fine gravel-sized limestone spalls, several bone fragments (Fig. 4E and F), some (molluscan) shell fragments and quartz sands, commonly etched (Fig. 4C and D), and the occasional (plant) ash (Fig. 4H) likely associated with the spalls and gravel clasts noted around this region during field sampling (Supplementary Table 1).

Mf 8c, distinguished by a spongy microstructure (Table 1), is annexed at the top of MM3B and in two thirds of MM3A (Fig. 4A; Fig. 4B). Etched, stained and micritised features on many of the calcareous clasts in the sediment suggest that these are heavily weathered through microbial activity, often in damp conditions (MacIntyre and Reid, 2003). Dissolution is apparent and widely occurring in mf 8c, demonstrated by casts of organic pseudomorphs (Fig. 4G) and localised illuviation and staining of Fe-rich clays from the overlying microfacies (mf 8d) evident under dark field light. Similar to coarse sediments in mf 8b, these coarse sediments also dip downslope towards the cave wall.

Mf 8d occupies the top third of MM3A (Fig. 4B). Here, the inclusions of Mn nodules and etched calcareous clasts in the speckled clays, and prevalence of Fe oxide staining (Fig. 4I) indicate that these sediments formed in a largely redoximorphic environment (Vepraskas et al., 2018). The weakly speckled clays (calcareous groundmass) coating rounded quartz sands (Fig. 4J) imply that these sands were likely reworked in the chamber from around the cave environment.

4.1.3. Interface between unit 8–7 (MM2C)

Sediments at the interface between Units 8 and 7 were deposited some time before ~24–12 ka (Fig. 2; Table 1). The interface is observed at the top of MM2C (Fig. 5A) and the base of MM2B (Fig. 5B), with their boundary being distinguished by a sharp bounding plane clearly seen under cross-polarised light (Fig. 5C).

In-situ blocky peds of vesicular-vughy silty clays separated by planes and channels comprise mf 8e (Table 1). Here, coarse inclusions are restricted mostly at the top along with mottling of Fe and Mn oxides. Unlike thin sections detailing the lower regions of Unit 8, bone and microcharcoal are less obvious in the sediment as both are very fine. Bones are also heavily phosphatised, although still structurally preserved (Fig. 5D and E). The largely isotropic nature of the groundmass (Fig. 5C) and some phosphatised individual components in the reddish brown silty clays (Fig. 5E–J) suggests that sediments in mf 8e are primarily organic.

4.1.4. Unit 7 (MM2B)

MM2B (Fig. 5B) details Unit 7, described in the field as pale yellow silts (Supplementary Table 1). Unit 7 is characterised by a single microfacies, mf 7 (Table 1), estimated to have formed ~24–12 ka (Fig. 2; Table 1).Well-developed planar voids and cracks help to distinguish the cross-laminated clayey silts which form distinct individual crusts in mf 7 (Fig. 6 A). Here, the micro-aggregates of rounded sandy clays in the laminations are likely rip-up clasts derived from the underlying microfacies since they display similar composition to sediments in mf 8e. Mn nodules, and a few microcharcoal and bone (Fig. 6C–G) comprise the rest of the coarse component in these silts, which also likely form part of underlying eroded substrate.

In thin section, the pale-yellow silts described during field sampling (Supplementary Table 1) is greenish-yellow undifferentiated clay exhibiting low birefringence. These are characteristic of sediments that are decalcified and phosphatised, which suggest that the sediments were likely waterlogged (Van Den Berg and Loch, 2000). Fe-rich clay lenses intercalate the phosphatised clays. In many areas, these clays are distinguished by the differences in their fabric. Fe-rich intercalations have coarser inclusions compared to those in phosphatic clays (Fig. 6B),

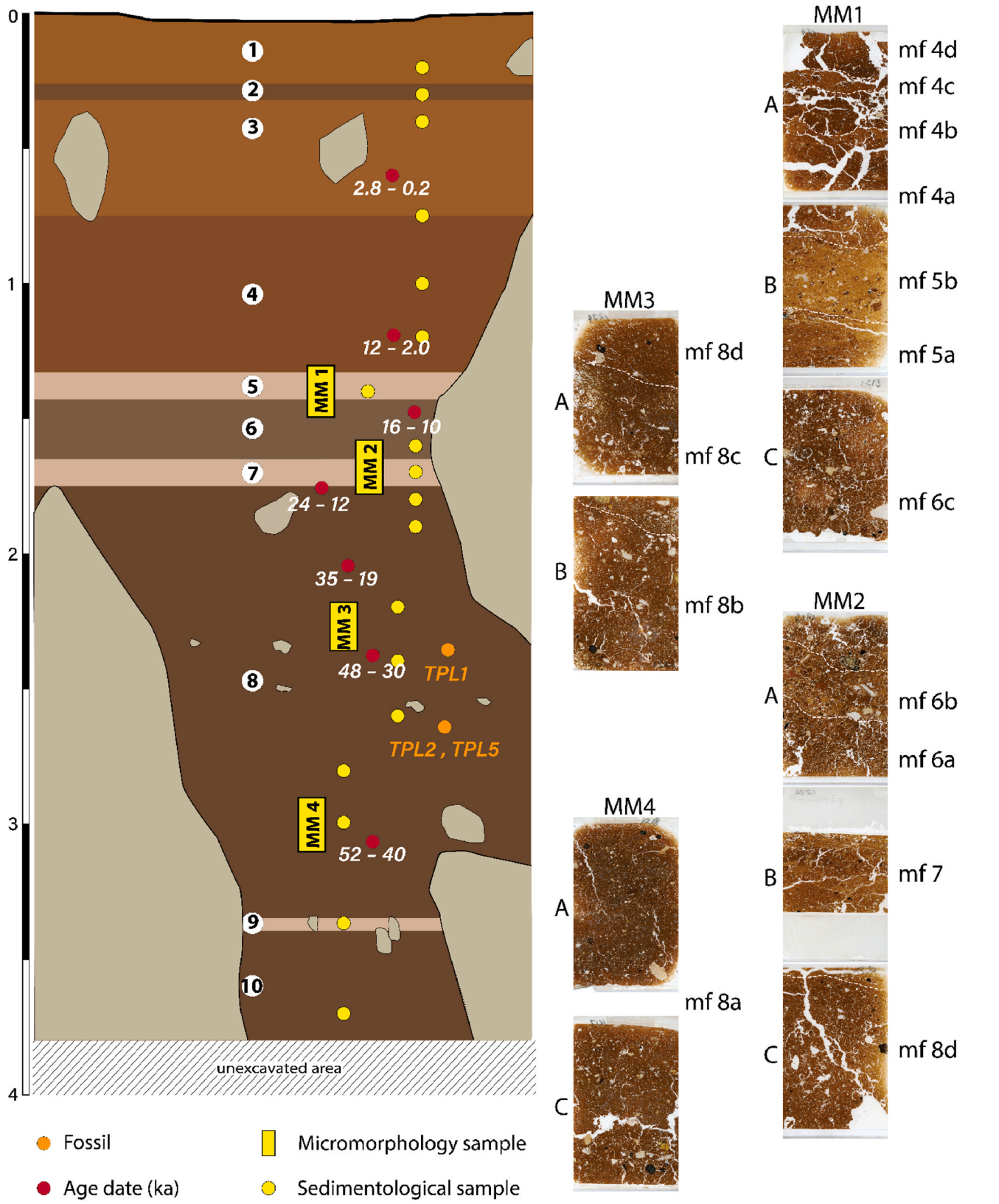

Fig. 2. **(Left)** Locations of the samples analysed, depositional age dates and human fossils from the upper 4 m of the sediment sequence at TPL. **(Right)** The ten thin sections and fifteen microfacies (mf) identified. Age dates are the 2σ modelled age dates reported by Freidline et al. (2023).

ARTICLE IN PRESS

Table 1
Microstratigraphic (micromorphological) characteristics of TPL Units 4–8 and identified microfacies, with their indicated depositional processes and interpreted depositional environments. Age dates are 2σ modelled dates reported by Freidline et al. (2023).

Unit	Age (ka)	Thin section	Micro-facies	Micromorphological characteristics	Process	Environment
4		MM1A	4d	Very poorly accommodated plane separated angular blocks, massive microstructure, common vertical planes, very few vesicles, sand-sized limestone fragments (common), shell fragments, Mn nodules, and amorphous micritic calcite nodules (few), poorly sorted in reddish brown speckled clays and calcite.	Colluviation (wet) and crusting	Dominantly arid cave conditions but with pronounced periods of (seasonal) wetting and occasional roof fall
			4c	Compact, massive microstructure with common chamber and few planar voids, calcareous sands (abundant), moderately sorted in yellowish brown undifferentiated clay, chamber containing rip up clasts		
			4b	Open microstructure, amorphous angular plates, common planar voids, few vesicles, calcareous coarse sands and limestone fragments (common), Mn nodules, microcharcoal and shell fragments (few), poorly sorted in reddish-brown weakly speckled clay, compression features between 4b and 4a.	Roof fall or trampling (?), Colluviation (wet) and crusting	
		MM1B	4a	Planar-channel microstructure, few vesicles and planar voids, limestone fragments and calcareous sands (frequent), shell fragments and Fe-rich clay clasts (few), moderately sorted in brownish yellow weakly striated calcite and undifferentiated clay, few crumb pellets in voids.	Bioturbation	
5			5b	Compact massive microstructure, dominant subrounded Fe-rich clay clasts, calcareous sands and amorphous micritic calcite nodules (frequent), bone fragments (variable preservation and oxidation) (common), microcharcoal (well-preserved), shell fragments and plant matter (weathered)(few), moderately sorted undifferentiated low birefringent greenish yellow clays.	Alluvial sedimentation and crusting	Temperate and relatively stable surface conditions with frequent low energy water-lain sedimentation and occasional input of combustion biproducts
	16–10		5a	Compact, rare planar void (horizontally oriented), calcareous sands (frequent), shell and bone fragments, microcharcoal (common), moderate–well sorted in intercalated microlaminated striated birefringent clays and calcareous silts (low birefringence), neoformed calcite in planar void, charcoal (~10 mm) compressed (horizontally) between interface of 5a and 5b.		
6		MM1C MM2A	6c	Moderately compact vesicular-planar microstructure, frequent vughs, common chambers (in-filled), Fe-rich sub-angular clay clasts (frequent), limestone spalls and fine gravels (common), microcharcoal (well-preserved) and micritic calcite nodules (phosphatised)(few), poorly sorted silty clay cross-striated b-fabric, localised areas of more compact vesicular-vughy microstructure undifferentiated b-fabric with mineral neo-formation (sparite), chamber in filled with crumby (organic) sandy clays.	Colluviation (dry) and bioturbation	Temperate and often damp cave conditions with frequent reworking of combustion biproducts and exogenous sediments on a relatively stable surface
			6b	Compact vughy-vesicular microstructure with well-accommodated amorphous sandy clay aggregates (vesicular-planar microstructure), partly slaked Fe-rich (subangular) clay clasts (frequent), slaked calcareous clay clasts, angular limestone spalls, angular quartz, shell and phosphatised bone fragments (common), phosphate-rich nodule (coprolite?) (very few), moderately sorted circular b-fabric (low birefringence), sloped bedding (~10°) towards cave wall.	Colluviation (wet)	Becoming humid in the cave with occasional reworking of sediments in aqueous media
			6a	Moderately compact vesicle and vertical plane microstructure, calcareous sands Fe-rich subangular clay clasts (coarsening up sequence) (frequent), moderately to well-sorted in mosaic speckled clay.	Colluviation (dry)	Semi-arid cave conditions with consistent input of comminuted cave sediments and eroded clays clasts
7	24–12	MM2B MM2C	7	Plane separated (well-accommodated) cross-bedded lamina (~5 mm), moderately compact vesicular structure with common planar voids, frequent (rounded) Mn nodules and staining, Fe-rich clay clasts (rounded), common fine gravel-sized (subrounded) limestone fragments, bone fragments (variable preservation), very few microcharcoal, moderately sorted in greenish-yellow weakly striated (parallel to cross-bedded orientation) undifferentiated clays (phosphate-rich), rare angular clayey silt clasts (low to no birefringence/isotropic).	Colluviation (wet) and crusting	Semi-arid cave conditions, possibly with frequent cave attrition and surface weathering during dry periods, and seasonal water-lain deposition coming from different areas of the cave during wet periods
8			8e	Channel separated compact blocks, vughy vesicular microstructure, occasional chambers (~5 mm dia.), frequent fine gravel-sized angular limestone fragments, common coarse sands (quartz), Mn nodules and staining, shell fragments, bone fragments (phosphatised), very few microcharcoal (well-preserved), moderately sorted in reddish-brown undifferentiated clays.	Colluviation (dry) and bioturbation	Becoming arid in the cave, relatively stable surface conditions and occasional reworking of comminuted sediments

(*continued on next page*)

Table 1 (*continued*)

Unit	Age (ka)	Thin section	Micro-facies	Micromorphological characteristics	Process	Environment
		MM3A	8d	Compact, very few planar voids, shell and bone fragments (frequent), Mn nodules and calcareous nodules (common), localised areas of Fe staining towards the base.	Colluviation (wet)	Becoming humid (and warmer) in the cave with seasonal wetting and drying events resulting in (possible) roof fall and spalling, and reworking of sediments (slump action)
			8c	Spongy microstructure, common vughs and vesicles, quartz sands (clay coated), calcareous coarse sands (slaked) (frequent), fine gravel–coarse sand-sized limestone spalls (phosphatised) (common), micritic calcite nodules (phosphatised) (few), microcharcoal, and clay clasts (slaked) (very few), localised areas of decalcification and Fe staining of speckled clay, occasional secondary calcite formation in voids.	Slump action	
	48–30	MM3B	8b	Similar to MM4 but less compact and more frequent planar voids (sloped ~30° down towards cave wall), limestone spalls (frequent), coarse quartz sands (etched), bone fragments (variable preservation) (common),micritic calcite nodules (phosphatised) and shell fragments (very few).	Roof fall (?), spalling and colluviation (wet)	
		MM4A	8a	Similar to MM4C in microstructure and groundmass but more compact, and with more fines, frequent Fe and Mn nodules, micritic calcite nodules and microcharcoal (well-preserved) (common), sub-angular sparite coated clay aggregate.	Colluviation (wet)	Generally wet ground conditions in temperate cave environment, occasional drying resulting in cracks (planes) and precipitation of carbonates in voids. Periodic sheetflow under variable energies of fluvial sedimentation (but becoming weaker up sequence) with occasional input of combustion biproducts
	52–40	MM4C		Moderately compact vughy-vesicular microstructure, few vertical planar voids (well-accommodated), Mn nodules and oxides (frequent), angular limestone and speleothem (spall) fragments (common), amorphous micritic calcite nodules (few), shell fragments and bone fragments (variable preservation) (few), microcharcoal (well-preserved) (few), reddish-brown speckled clay, recurrent horizontal sand and gravel-sized stringers becoming finer up sequence, frequent clay coatings and occasional secondary carbonates (sparites) precipitated in void spaces.		

which is likely borne of the preservation conditions in phosphate rich and waterlogged environments common in tropical cave settings (McAdams et al., 2021).

4.1.5. Unit 6 (Thin section MM2A and MM1C)

Unit 6, described in the field as calcium carbonate and gravel-rich dark brown silty clays (Supplementary Table 1), was formed ~16–10 ka (Fig. 2; Table 1). The lower limits of Unit 6 are represented in thin section MM2A (Fig. 7A), while its upper limits are represented in thin section MM1C (Fig. 8A). Three microfacies are apparent in MM2A (Fig. 7A; Table 1): mf 6a, a graded and well sorted mosaic speckling of clays with a relatively open microstructure indicating a period of infrequent dynamic sedimentation; mf 6b, a moderately packed deposit of poorly sorted clay aggregates, shell and phosphatised bone fragments (Fig. 7F–I), a possible coprolite (Fig. 7E–G, H) and slaked calcite-rich clays (Fig. 7C) dipping down (~10°) towards the cave wall; and mf 6c, a poorly sorted deposit of amorphous blocks of vesicular-planar sandy clays capping the thin section.

Mf 6c also characterises the upper region of Unit 6, encompassed in MM1C (Fig. 7B). Here, mf 6c is dense, partly slaked, vughy vesicular silty clay with poorly sorted coarse sediment and crumb-like clay aggregates often packed in channels and chambers (Fig. 7D). Its course components include limestone spalls, Fe-rich clay aggregates, and fragments of microcharcoal and ash (Fig. 7J), which are well-preserved. In contrast, bone fragments are variably preserved (Fig. 7, F–I, K, L) with some showing signs of being calcined (Fig. 7F–I)

4.1.6. Unit 5 (Thin section MM1B)

Thin section MM1B covers Unit 5, a shallow pale-yellow silt layer that contains occasional fine calcium carbonates, likely formed during the Pleistocene–Holocene transition ~12 ka (Supplementary Table 1; Fig. 2). The boundaries between Units 6 and 4 are also documented in this thin section (Fig. 8A). Mf 5a is the Unit 6–5 interface, which is compact finely bedded sands and silts intercalated with yellow and reddish-brown clay laminae (Fig. 8B). A small number of noticeably coarse particles (>~2 mm) of charcoal, bone, and shell comprise these laminar accumulations, while the finely bedded sands and silts suggest sorting of coarse sediment, likely from mf 6c in MM1C (Section 4.1.5; Fig. 7B–D).

Based on SEM-EDS analysis (Fig. 8C), the pale yellow silts of Unit 5 encompassed in mf 5b are formed primarily of comminuted Ca-rich oo ids, mixed with feldspar clays (i.e., Al-silica rich), and to a lesser extent phosphorous (P). Phosphates in these sediments are likely residual from the frequently weathered bone (Fig. 8D–G) and some decomposing plant matter (Fig. 8H). The rounded clay clasts in mf 5b are probably reworked from mf 5a, noting similarities in their Fe-rich clay component and those in the upper region of Unit 6 (Section 4.1.5; Fig. 7). These 'rip-up clasts' are mostly cracked. They are comparable to baked clays (Tsatskin and Gendler, 2016: 288), likely exposed to temperatures of ~200–400 °C (Fig. 8I, Ferro-Vázquez et al., 2022: 291) and often occur alongside bone fragments that have likely been burnt or that have been calcined (Fig. 8D and E; Mentzer et al., 2014).

4.1.7. Unit 4 (Thin section MM1A)

The base of Unit 4 is captured in MM1A and is formed of silty clays probably deposited ~12 ka and later (Fig. 2; Table 1). Distinct microstructures help distinguish four microfacies in the thin section (mf 4a–d), described from the base up. Mf 4a has a dominantly channel microstructure indicating its largely bioturbated nature. This feature is also partly seen in the upper part of MM1B. The matrix of mf 4a is formed of compact, undulating, and intercalated microlaminations of Fe-rich clays and phosphatised calcareous fine sands and silts (Fig. 9A). Closer examination shows that the calcareous laminations are moderately slaked and composed primarily of ooids (Fig. 9B). Deformation features characteristic of compressed water-saturated sediment, usually from trampling (Karkanas, 2019) or typically formed during the mass

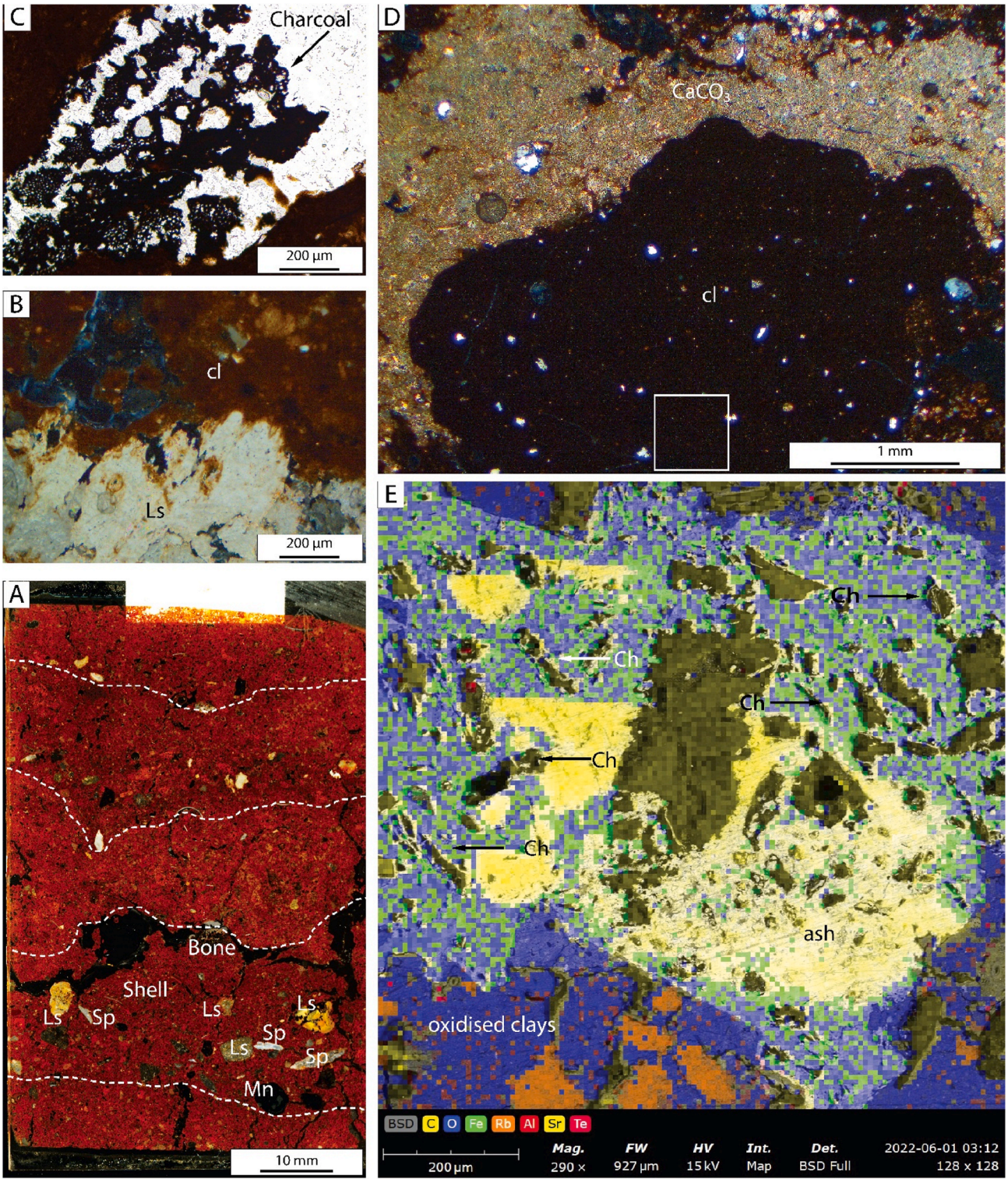

Fig. 3. **(A)** Macroscan of thin-section MM4C (dark field) with sediment stringers outlined and primary components of stringers labelled: Spalls (Sp), phosphatised limestone (Ls), and manganese nodules (Mn). **(B)** Clays (cl) coating etched limestone (Ls) (XPL) **(C)** Articulated plant cellular structure in microcharcoal from MM4C (PPL). **(D)** Calcite ($CaCO_3$) encrusted clay clast (cl) in MM4A (XPL). White box shows the general location of the EDS map analysis in panel 'D'. **(E)** EDS map analysis showing carbon and oxygen-rich micrite (ash) and fragments of microcharcoal (Ch) expressed as carbon-rich cracked elongated angular matter within iron and oxygen-rich clay minerals (Al, Te, and Rb).

movement of sediments (Bertran, 1993) are observed between 4a and 4b (Fig. 9C), where the Fe-rich clay coatings in its wide voids are indicative of often wet environments (Fig. 9D). A compact, vesicular lens of partly phosphatised moderately sorted calcitic sandy silt (Fig. 9E) forms mf 4c, which almost entirely caps mf 4b. Similar to microstratigraphic features in Unit 5 (Section 4.1.6; 8) rip-up clasts are also present. They are however fewer and larger in dimension, well-accommodated but highly separated, and with sparry calcite precipitated within vesicles, likely formed during arid cave conditions (Fig. 9F; Zamanian et al., 2016). Vesicular massive blocks of Fe-rich sandy clays (Fig. 9G) moderately

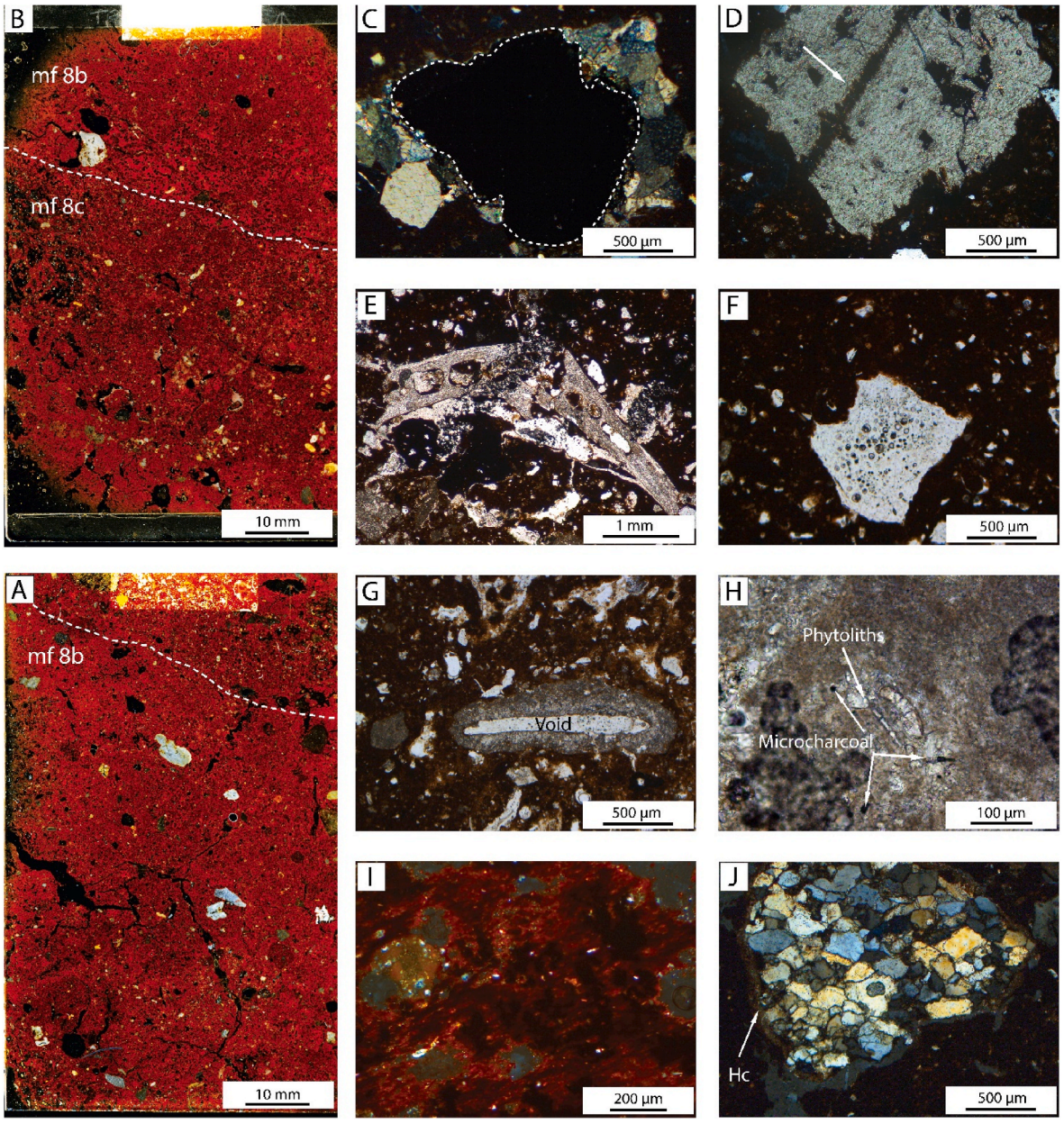

Fig. 4. (**A**) Macroscans of thin section MM3B, and **(B)** thin section MM3A (dark field). Note Fe-rich clay (bright red) accumulations in several horizons and within interstitial void spaces and decalcified regions in mf 8b **(C)** Dissolution features in quartz sand. Outline indicates the void created by the dissolution of the grain (XPL) **(D)** Severely etched quartz sand. Arrow indicates the etched feature on the grain (XPL) (**E**) Fragmented bone (PPL). (**F**) Etched bone fragment (PPL). (**G**) Sparite mould on void, possibly bone pseudomorph. A dissolution feature. (**H**) Phosphatised micrite with phytoliths and microcharcoal (PPL) – plant ash. **(I)** Fe-enriched clays in mf 8d. **(J)** Speckled clay (hypo)coating (Hc) rounded quartz (XPL).

sorted in discrete horizontal beds (Fig. 9H) form mf 4d. Considering the characteristic capacity of clays to swell and shrink and compaction of the sediment from which MM1 was sampled (Supplementary Table 1), the well-accommodated but highly separated block structure of mf 4d is likely an artefact of the drying process during sample preparation.

4.2. Magnetic susceptibility and loss-on-ignition

The results of the χ and LOI analyses, provide information about sediment provenance and delivery to TPL, and help to infer its ground conditions (Fig. 10, Supplementary Table 2). These results are interpreted with reference to the microstratigraphy.

The χ of sediments is generally increasing up-profile (3.7–0.2 m) but shows a marked change through the lower part of the sequence (3.7–1.8 m) between Unit 9–7 and periodic alternations across the upper sequence (1.7–0.2 m) between Units 6–1 (Fig. 10). Throughout most of the sequence, carbonate (CC) and organic values (OM) show positive correlation (0.852) with each other and negative correlation with χ (-0.482 for OM and -0.532 for CC), suggesting that autogenic and allogenic sediment sources contributed equally to site formation for much of its depositional history.

The high χ values of Unit 8 are indicative of episodes of wetting and drying of cave sediments (Maher, 1998; Evans and Heller, 2003: 94), and potentially burning (Tite and Mullins, 1971; Lowe et al., 2016) rather than soil formation, which is unlikely in deep cave settings such as TPL. This result is consistent with the recurring laminae of sandy and silty clays, and the well-preserved biproducts of combustion recorded in thin sections representing Unit 8 (Section 4.1.1; 4.1.2; Fig. 3; Fig. 4).

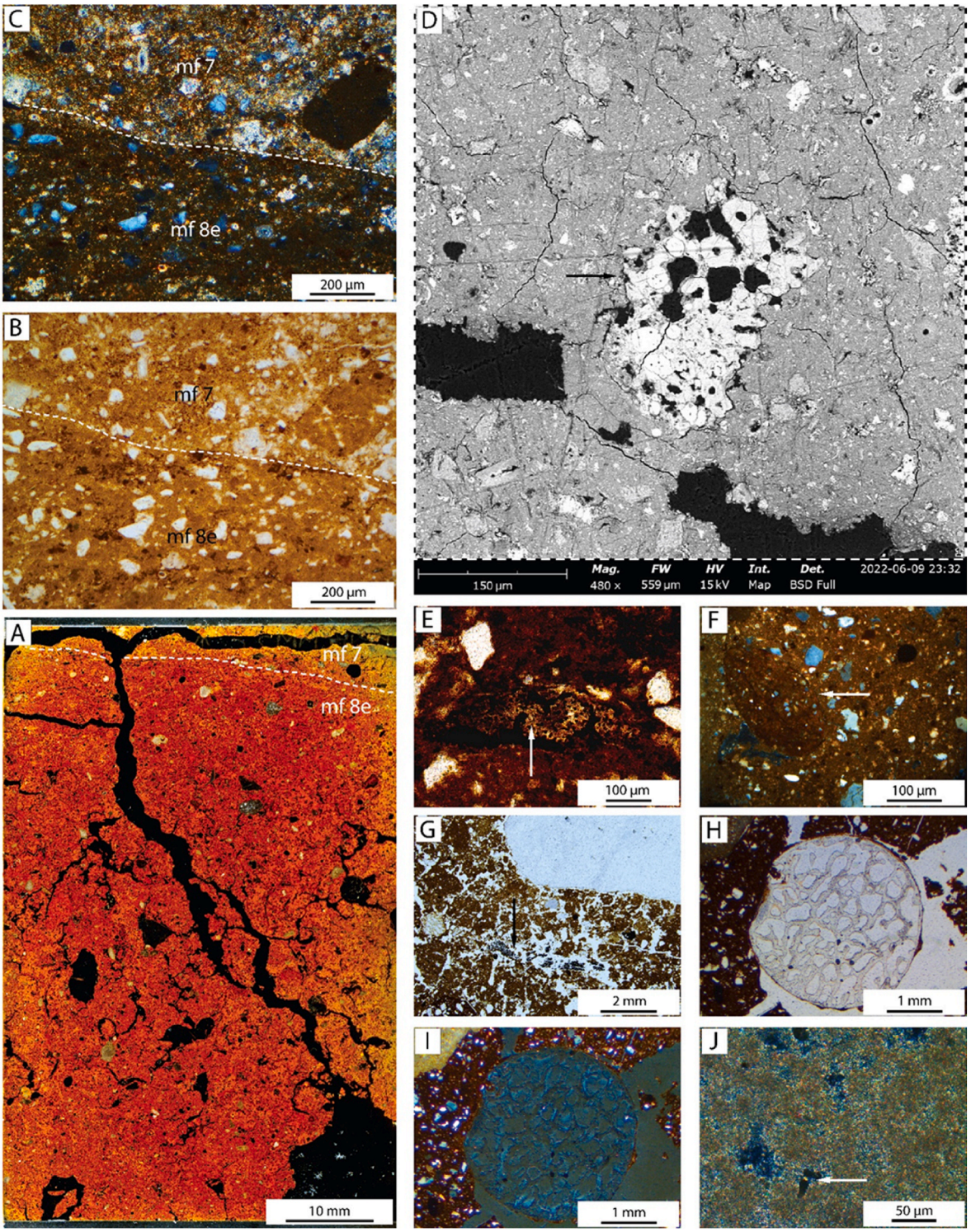

Fig. 5. **(A)** Macroscans of thin section MM2C (dark field). Dashed line defines the boundary between Unit 8 (mf 8e) and 7 (mf 7). **(B)** Boundary between mf 8e and mf 7 in closer view (PPL). Note the difference in coarse fractions of sediment. **(C)** Same as 'B' (XPL). Note the similarity of fine fraction of dark clast in mf 7 with fine fraction in mf 8e. **(D)** Backscattered electron (BSE) image of trabecular bone fragment indicating severe mechanical (and chemical) weathering. **(E)** Phosphatised trabecular bone fragment (XPL). **(F)** Subrounded clay clast (XPL). **(G)** fragmented charcoal (PPL). **(H)** (Thinly) clay coated trabecular bone (PPL). **(I)** Same as 'H' (XPL). **(J)** Microcharcoal in phosphatised micrite – ash.

Considering this, fluctuations in χ from Units 6–1 suggest seasonal wetting and drying of the cave sediments, with periods characterised by either extreme saturation or desiccation inferred from diagnostic features identified in thin sections from Unit 6 (Section 4.1.5; Fig. 7) and the base of Unit 4 (Section 4.1.7; Fig. 9).

The χ value in Unit 4 at ~0.75 m is most likely a result of burning as fine bands of micro-charcoal overlain by white flecks of sand were recorded in the section during field sampling (Supplementary Table 1). The carbonate values and increase in χ at this level, suggest that these white flecks are ash (Canti, 2003; Woods, 2003: 10), possibly formed from either a continuous or single intense combustion of charred wood and associated decline of organic matter in the sediments (Mallol et al.,

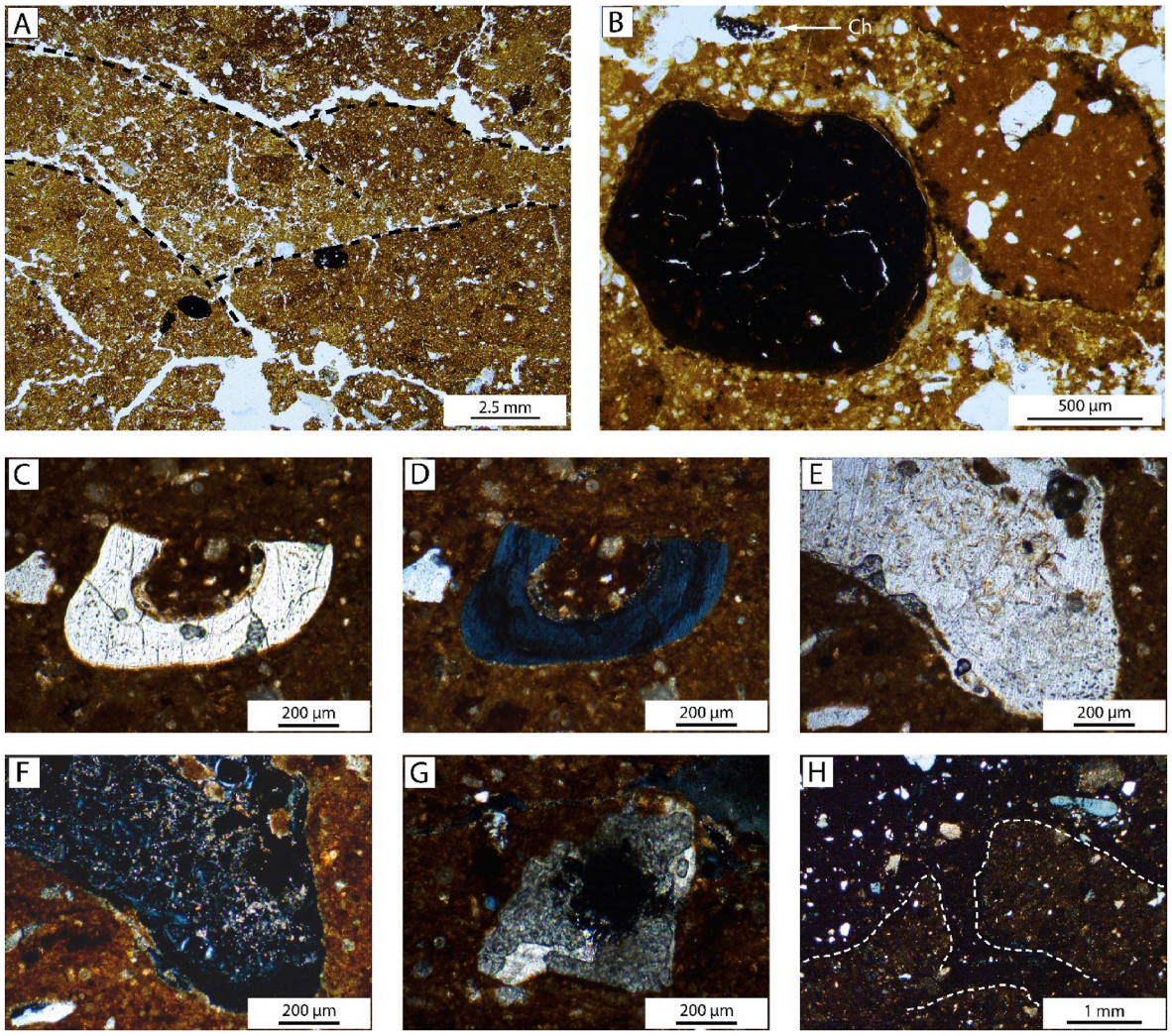

Fig. 6. (**A**) Discreet cross laminations of clays and silts in Unit 7 (mf 7) defined by dashed lines (PPL). **(B)** Rounded manganese-stained clast and Fe-rich clay clast suggesting reworking and mixing of materials from different depositional environments. Charcoal (Ch) is noted (PPL). **(C)** Bone fragment (PPL). **(D)** Same as 'C (XPL). Note the dull grey colour indicating calcination (Mentzer et al., 2014) **(E)** Heavily weathered bone (PPL). Note haversian canals in lower region. **(F)** Same as 'E' (XPL). Note the dull grey regions and micrite speckling indicating recalcification or calcination. **(G)** Dissolved quartz (XPL). **(H)** Angular clayey silt clasts (outlined) within sandy clay matrix (XPL). Note the partly isotropic nature of the clasts suggesting decalcification and phosphatisation.

2017: 300). Similar correlative relationships between the values of OM, CC and χ are also observed in the lower region of Unit 8 (3.0 m), and in Unit 6 (1.6 m), with micro-traces of combustion biproducts commonly noted in thin sections MM4A (Fig. 3C–E), MM2A, and MM1C (Fig. 7, F–I, J). These correlative relationships suggest that both the depositional environment and burning events influenced the χ of sediments deposited during MIS 3 (~52–30 ka), towards the end of the Pleistocene (~16–12 ka), and in the later Holocene.

5. Discussion

The microstratigraphy and bulk geochemistry of the upper 4 m of the sediment sequence in TPL allow us to develop a more nuanced understanding of the depositional history and on-site ground conditions of the cave from ~52 to 10 ka (Section 5.1); elucidate the taphonomic history of the *TPL1*, *2* and *5* human fossils in relation to the depositional history of the cave (Section 5.2); and identify micromorphological features that serve to demonstrate TPL as a unique and important site to better understand the evolution and dispersal of *Homo sapiens* in the Far East (Section 5.3; 5.4). Together, these discussions underscore the potential for a micro-geoarchaeological approach to the study of archaeological and fossil sites in SEA (Morley, 2017; Morley et al., 2023).

5.1. The changing environments of Tam Pà Ling from ~52 to 10 ka

This microstratigraphic study examines in detail the model of 'low-energy slope wash' depositing sediments (and fossils) in the upper 4 m sediment sequence in T3. By combining the microstratigraphy with the χ and LOI data we can refine the interpretation of the depositional environments in the cave from ~52 to 10 ka.

5.1.1. Basal unit 8, MM4 thin sections: wet colluviation in temperate conditions (~52–40 ka)

The coarse stringers suspended in interbedded clay and silt laminations suggest regular deposition of sediment out of suspension in slow moving water ~52–40 ka (Section 4.1.1; Fig. 3A). The moderate to well sorted composition of the stringers, and the grading of fine laminated sediments indicate that deposition was low (slackwater or ponding) and sometimes slightly higher energy decreasing over time, leading to drier conditions. The χ values in lower Unit 8 correspond to the sediments recorded in MM4 thin sections (Section 4.2; Fig. 10) and support these microstratigraphic interpretations. The frequent sand- and gravel-sized limestone clasts in MM4 thin sections reflect the larger contribution of autogenic sediments in the cave. Direct correlation between the values of χ and carbonates at 3.0 m of the sequence corroborates this

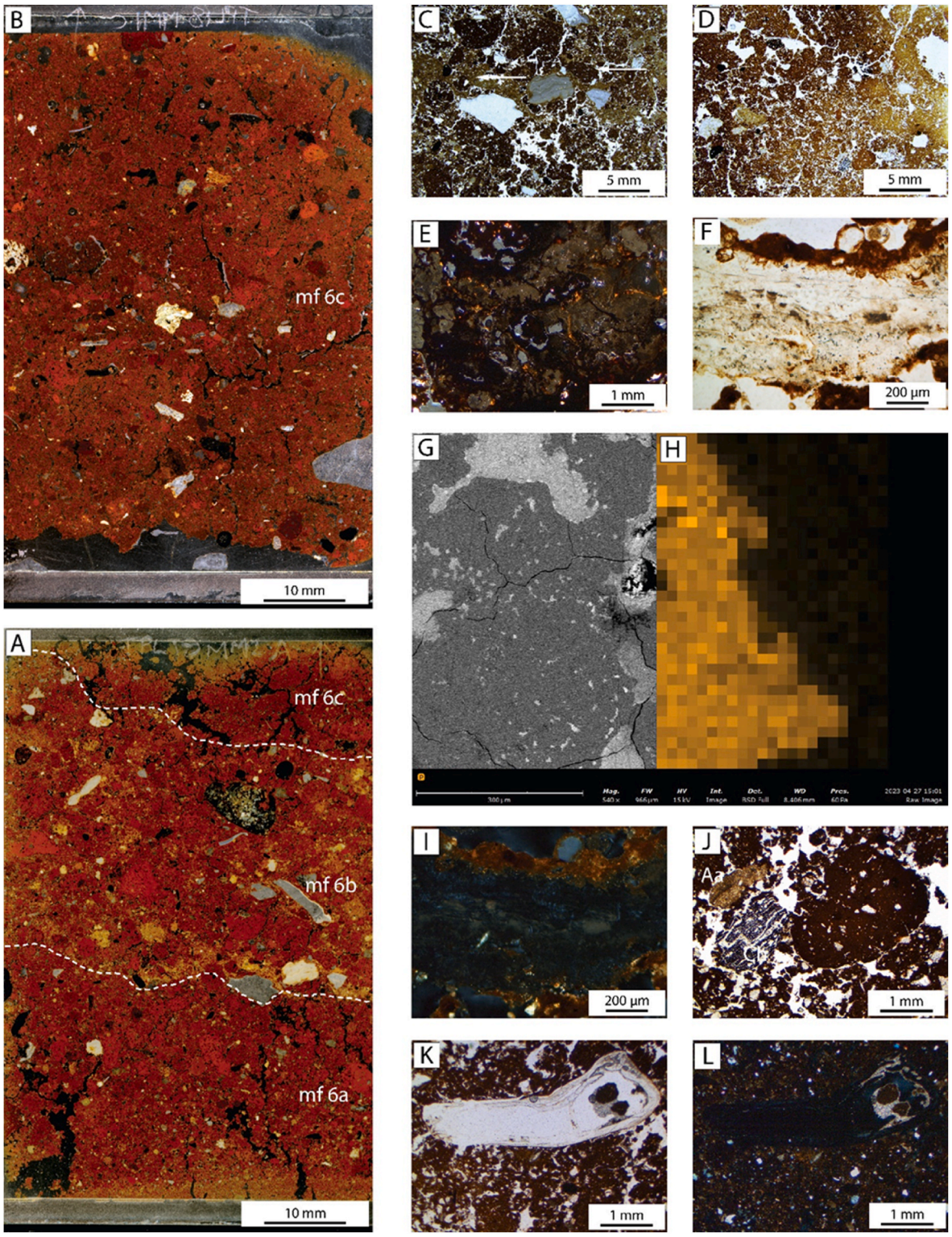

Fig. 7. (**A**) Macroscan of thin section MM2A and **(B)** MM1C (dark field). **(C)** In mf 6b: slaked (yellowish green) sediment formed interstitially within voids (PPL). **(D)** In mf 6C: Heavily turbated upper region of MM1C (PPL). **(E)** Amorphous isotropic clay mass in mf 6b (XPL). Note the low-birefringent characteristic of clays indicating it as phosphate-rich sediment, likely coprolite. **(F)** Heavily weathered, clay coated bone fragment (PPL). **(G)** BSE image of a region of 'E'. **(H)** EDS map highlighting phosphate-rich sediment (orange colour). **(I)** Same as F (XPL). Note the dull grey and yellowish green regions in the bone suggesting possible calcination and phosphatisation (Mentzer et al., 2014). **(J)** Close stratigraphic association of Fe-rich clay clast, charcoal (Ch), and ashy aggregate (Aa) in mf 6c. **(K)** Decalcified bone (PPL). Note haversian canals. **(L)** Same as 'K' (XPL). Note the absence of ropy structure.

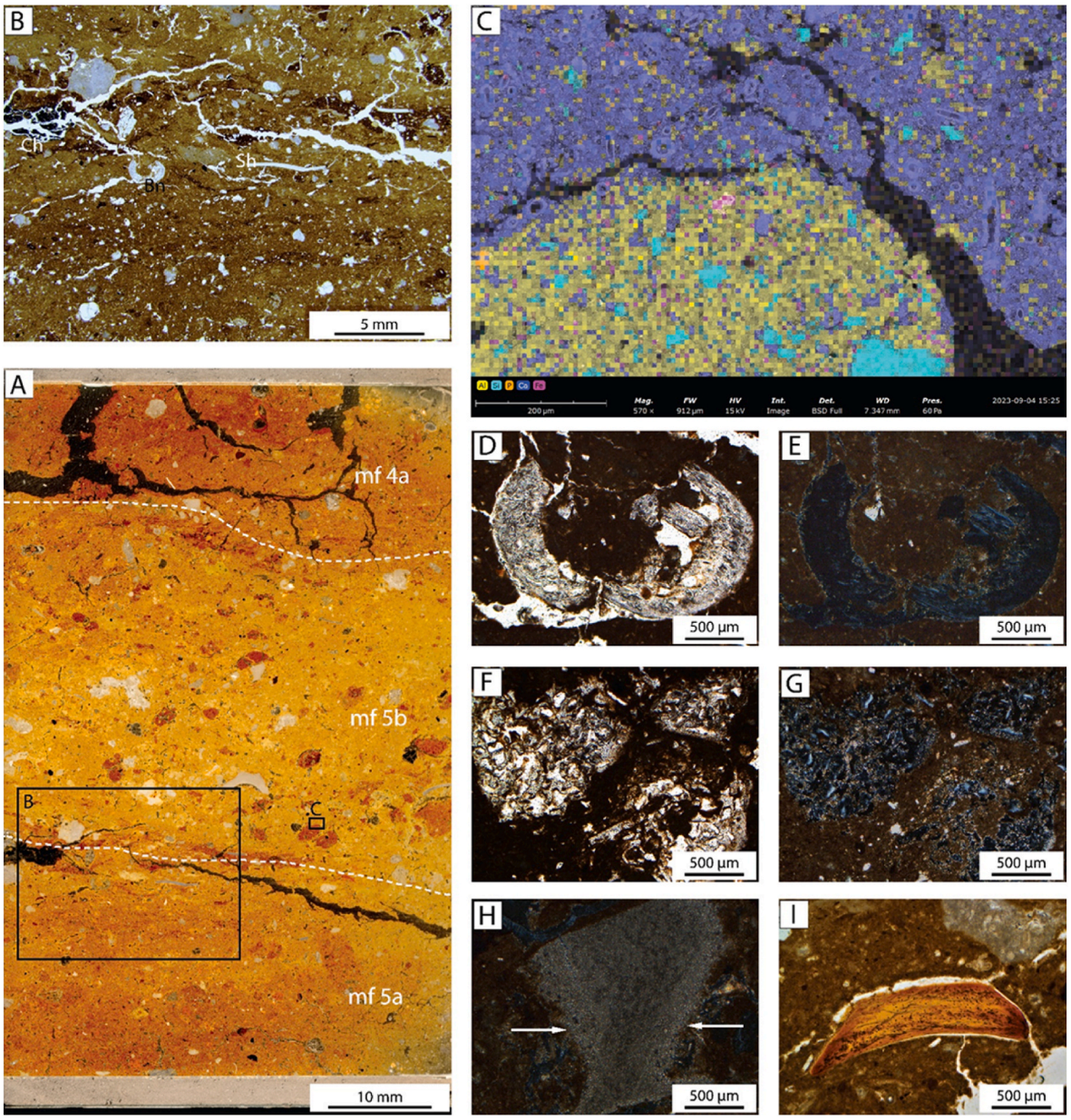

Fig. 8. (**A**) Macroscan of thin section MM1B (dark field). Large rectangle is magnified in 'B', while the small rectangle is analysed under SEM-EDS in 'C'. **(B)** Finely bedded sands and silts intercalated with yellow and reddish-brown clay laminae (PPL). Note the horizontal orientation of coarse sediment such as microcharcoal (Ch), shell fragments (Sh) and bone (Bn). **(C)** SEM-EDS map analysis showing some of the Fe-rich rip-up clasts in the phosphorous and calcium-rich silts and clays of Unit 5. **(D)** Weathered bone (PPL) **(E)** Same as 'D' (XPL). Note the similar structure of the bones in PPL, and their difference in XPL. The ropy structure of bone in under XPL is dull grey and only partly preserved, suggesting that is has been calcined (Mentzer et al., 2014). **(F)** Trabecular bone (heavily weathered) (PPL). **(G)** Same as 'F' (XPL). Note the (calcitic) speckling, suggesting replacement of bioapatite in bone by calcite, likely after decalcification. **(H)** Plant pseudomorph. Note the internal reaction rims and physical rupturing of edges, suggest that it is physically and chemically decomposed. **(I)** Bone oxidised in high temperatures, suggested by its reddish hue. Note haversian canals partly stained in MnO2.

(Supplementary Table 2, Fig. 10). The Fe-rich groundmass with occasional reduction features (i.e., typic MnO2 nodules) reflect the deposition of secondary Mn and Fe oxides from the cave entrance (Freidline et al., 2023), correlating with the increase of χ values in sediments ~3.4–2.8 m (Section 4.2; Fig. 10). Together, the data suggest that it is mostly silts and clays that wash in from the entrance of the cave, only later picking up comminuted cave sediments and other larger detritus already inside the cave, moving down slope towards T3.

The reconstructed ground conditions at TPL ~52–40 ka (Section 4.1.1, Fig. 3) do not correlate with climatic conditions seen in the region. Yamoah et al., (2001) show from their analyses of lake sediments that during mid MIS 3 (~48–36 ka) El Niño-like conditions led to intense aridity over SEA beginning ~45 ka. The severely arid conditions they suggest only later changed ~36 ka due to more frequent rains. In MM4 thin sections, the dense structure of sediments, frequent redoximorphic features, and the recurrent sediments stringers that grade up sequence also observed in other prehistoric cave sites such as at Tabun in Israel (Goldberg, 2001; Friesem et al., 2021) indicate a frequently wet cave environment. However, the occasional crystalline void fills show that conditions were sufficiently dry to accelerate the evaporation of carbonate-charged water in the cave (White, 2007), but not hot enough to form more open sedimentary structures such as poorly accommodated void spaces. Considering these, our reconstructed cave conditions suggest that ~52–40 ka rainfall was regular in at least this region of the

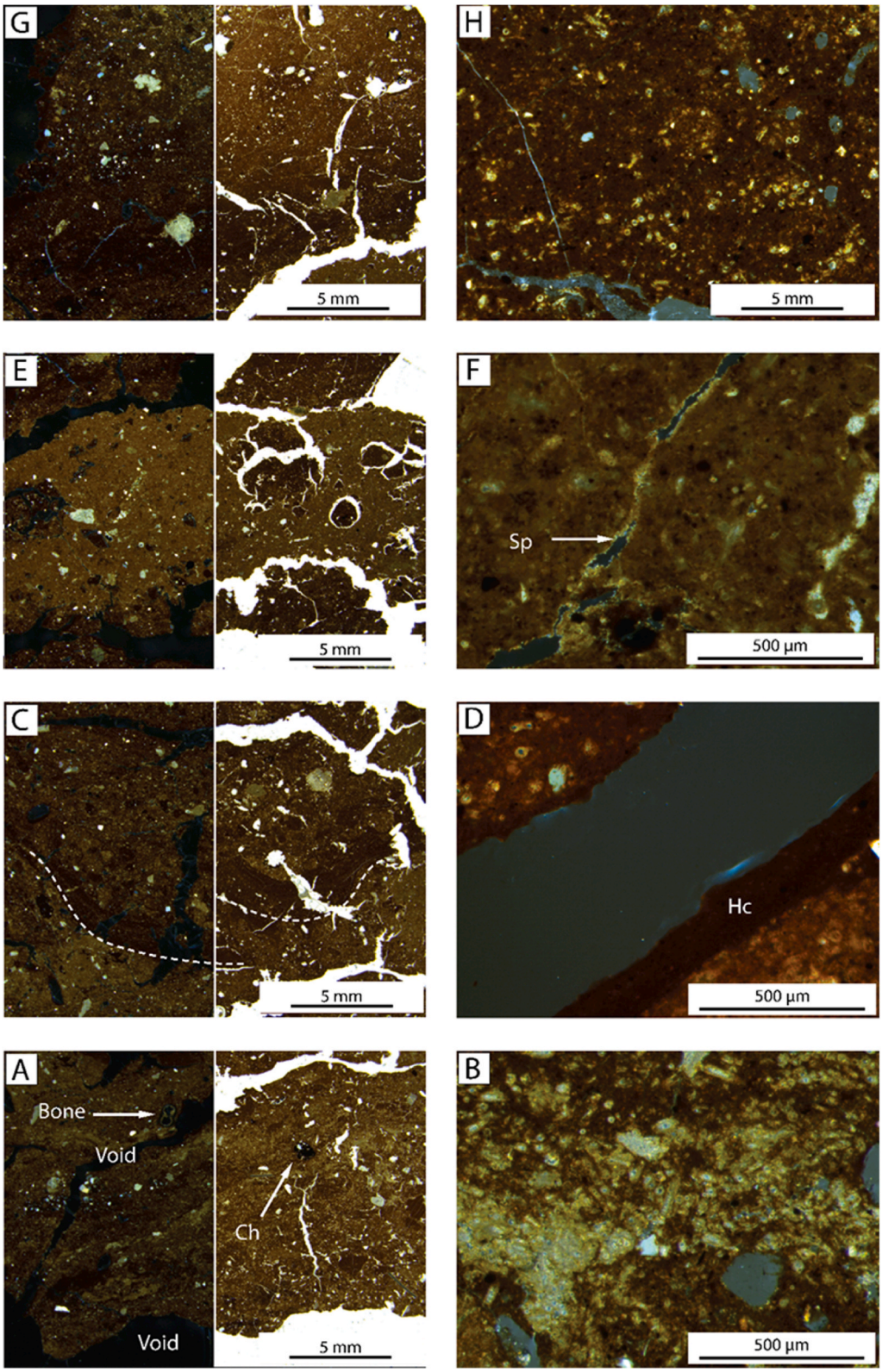

Fig. 9. (**A**) mf 4a: Fissured compact, undulating, and intercalated microlaminations of clays and fine sands and silts in XPL (left side) and PPL (right side) interrupted by channels. Bone and charcoal are noted. Third order birefringence on clays suggests it is Fe-rich. **(B)** Partly slaked ooids (XPL). Note the low order birefringence indicating that these sediments are also partly phosphatised. **(C)** mf 4b: Phosphatised silts with poorly sorted calcareous sands and clay clasts overlying finely laminated and compacted Fe-rich clays in XPL (left side) and PPL (right side). Thrust planes – upwardly curving disjointed clay lamina (outlined) indicating downward slope movement – are noted (Bertran, 1993: 658). **(D)** Illuviated clay (hypo)coating (Hc) in voids (XPL). **(E)** mf 4c: Compact, vesicular lens of moderately sorted sandy silt in XPL (left side) and PPL (right side). Isotropic silts in XPL suggests it is phosphatised. Note the cracked and poor accommodation in voids of the rounded rip-up clasts in the matrix. **(F)** Sparite (Sp) formation within vesicles and fissures within the matrix (XPL). **(G)** mf 4d: Angular block of Fe-rich sandy clays with very discreet horizontal banding in XPL (left side) and PPL (right side). **(H)** Ooids comprising the sandy component of the matrix (XPL). Note their moderate separation and chaotic distribution within clays suggesting weathering either from spalls or cave walls and ceiling.

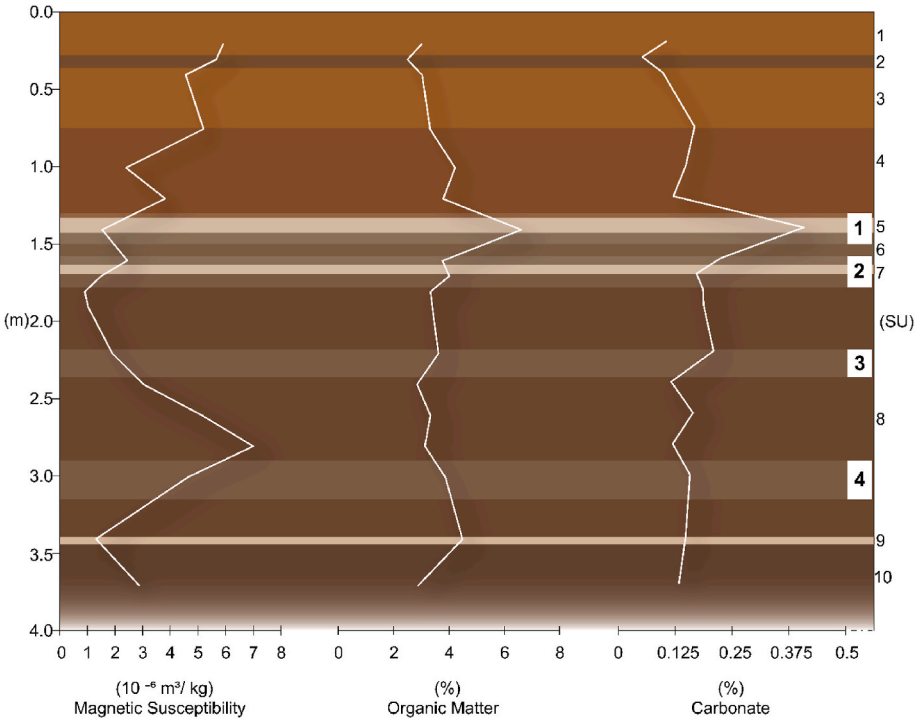

Fig. 10. Magnetic susceptibility, organic matter and carbonate content determinations from the upper 4 m of sediment sequence at TPL. Y-axis shows depth in metres (m) below excavated surface level. Stratigraphic units (SU) are labelled on the right. Enumerated black boxes represent micromorphological block samples MM1–4.

AMR, and that ambient conditions in at least the cave was temperate. These conditions are corroborated by other research from TPL (Milano et al., 2018; Freidline et al., 2023; McAllister-Hayward et al., 2024) and research in the narrow mountains of the region that highlight elevation as a significant landscape feature that contributes to moderating climatic conditions (Wu et al., 2016; Rabett et al., 2017). Combined, the research suggests that regular rains and closed forests around the Pa Hang karst tempered the dry (and hot) conditions in the region and muted humidity inside the cave ~52–40 ka.

5.1.2. Upper unit 8, MM3 thin sections: cave attrition and wet colluviation (~48–30 ka)

The poor sorting of coarse sediments deposited on down-sloped surfaces and the orientation of cracks seen in MM3 thin sections (Section 4.1.2; Fig. 4) suggest that there was mass wasting of sediments from the chamber area towards the cave wall ~48–30 ka. The deposition of these sediments may have been penecontemporaneous due to the lack of clear bounding surfaces between mf 8b–c (Fig. 4A). These deposits first occur as limestone spalls and gravel stringers (Supplementary Table 1), followed by poorly sorted clays and silts with fine gravel-sized limestone spalls (mf 8b, Fig. 4A), and finally by moderately sorted sandy clays and silts in mf 8d (Fig. 4B). Together, the features seen in MM3 thin sections are consistent with slumping, creating a topographic relief that is infilled by colluvial deposits (Martinsen, 1978; Bertran and Texier, 1999; Mücher et al., 2018). The coarse components in this upper region of Unit 8 are consistent with the increasing values of carbonates ~2.4–2.0 m in the sequence (Section 4.2; Fig. 10), indicating the significant contribution of autogenic cave sediments to these deposits, and suggest that these are derived from a period of cave attrition, even perhaps a ceiling collapse.

Fe-rich solute accumulations within interstitial voids and calcite-rich silt capping on sand grains recorded in MM3 (Fig. 4I and J) indicate illuviation, suggesting that ground conditions remained wet, such as we see in MM4 thin sections (Section 4.1.1; Fig. 3). The more open microstructure, occasional secondary crystalline formation within void spaces, and etched features on quartz sands and organic pseudomorphs in MM3 (Fig. 4C and D), when compared to MM4 thin sections, suggest that ambient conditions at this time were hot and humid and that the ground conditions were likely highly acidic. Etched dissolution features are notably formed in high temperature conditions (Howard et al., 1996; Sleep and Hessler, 2006), while the low values of χ (Section 5; Fig. 11) likely relate to dominantly acidic environments in the cave during this period (Maher, 1998; Evans and Heller, 2003: 87).

Our analyses of sediments in the upper part of Unit 8 indicate that the predominantly wet surface of the chamber had undergone a topographic change due to significant cave attrition following a shift from temperate conditions ~52–40 ka to warmer and more humid conditions ~48–30 ka. These conditions align with regional climate reconstructions indicating increased humidity and more frequent rains beginning ~36 ka (Yamoah et al., 2001; Marwick and Gagan, 2011) and previous sedimentological analysis of TPL suggesting that there was a possible collapse of the cave roof sometime between ~50–42 ka and ~36–30 ka (Freidline et al., 2023). Combined, the research suggests that cave and regional conditions significantly impacted ground conditions in TPL ~48–30 ka.

5.1.3. Unit 8–7, thin section MM2C and MM2B: marked shift from humid to semi-arid cave conditions during the LGM (~24–12 ka)

The developed blocks of vesicular vughy clays observed in mf 8e in MM2C (Section 4.1.3; Fig. 5A) differentiating the top of Unit 8 from the rest of its lower sequence suggest that conditions in the cave had become substantially drier. These features also suggest that sedimentation decreased enough to permit some bioturbation and formation of a sedimentary crust (Fig. 5B and C) just before ~24–12 ka (Fig. 2; Table 1). The crusting in mf7 observed in MM2C that helped to distinguish cross-laminations in this sequence (Section 4.1.4; Fig. 6) imply a continued aridity in the cave 24–12 ka (Fig. 2; Table 1). Although ground conditions in the cave were predominantly dry, sedimentation regularly involved colluvial (wet) deposition indicated by the cross laminations of phosphatised silts and organic clays with occasional well-preserved charcoal and decalcified bone fragments (Fig. 6A–D). This implies that the sheetflow deposition via small streams or rivulets

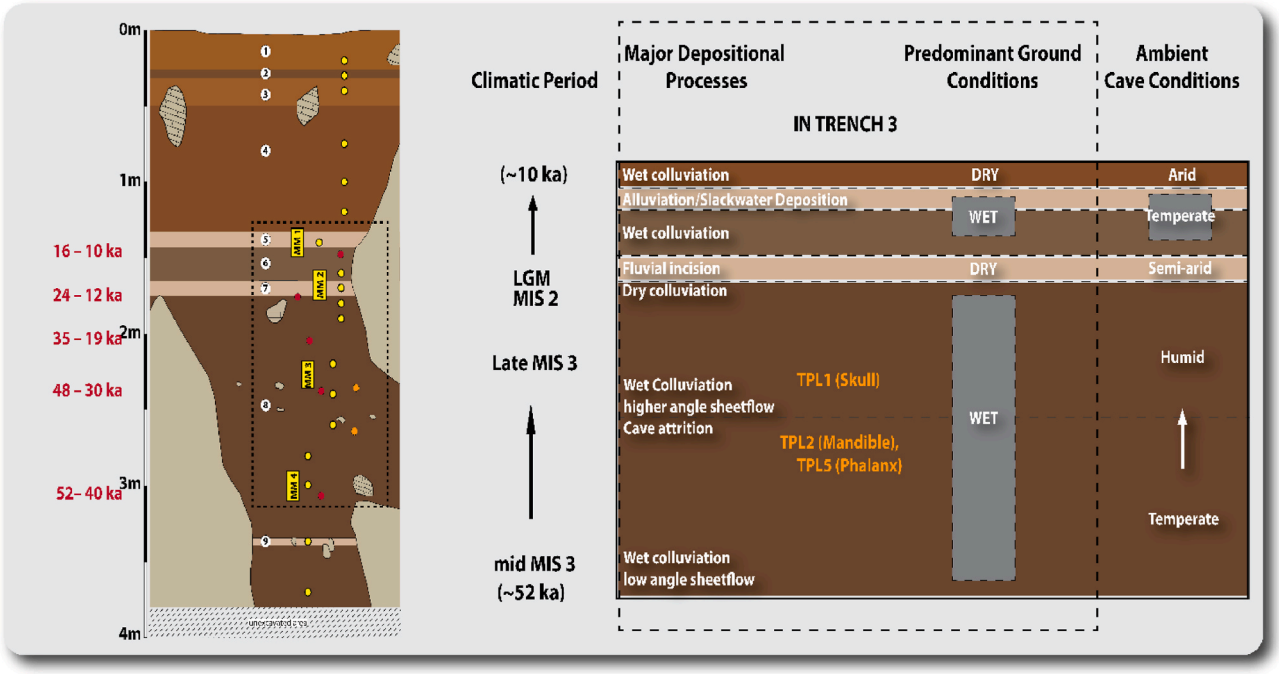

Fig. 11. Model outlining the major depositional processes and predominant ground conditions in T3 and the ambient conditions in TPL from ~52 to 10 ka.

derived from multiple directions, was possibly associated with seasonal rains. The fine cross-laminated silts in mf 7 suggests that depositional currents during the LGM were not as dynamic as observed in sediments from most of Unit 8 deposited during MIS 3 (Section 4.1.1–4.1.2; Fig. 3A; Fig. 4A and B), and that these phosphate-rich silts were likely often waterlogged and ponded (Van Den Berg and Loch, 2000). Together, these features suggest that conditions in TPL during the LGM were dry and received less input of water during monsoon rains than in MIS 3. The trend in χ, OM and CC from sediment samples in the interface between Unit 8–7 corroborate this interpretation (Section 4.2; Fig. 10). These semi-arid conditions in TPL are similar to those microstratigraphically reconstructed at cave sites in northern Vietnam and Thailand (McAdams et al., 2020; Saminpanya and Denkitkul, 2020), and therefore likely reflect the general climate around the region during the LGM.

5.1.4. Unit 6, thin section MM2A and MM1C: wet colluviation in temperate cave conditions between 24–12 ka and 16–10 ka

Mf 6a–c, encompassed in thin section MM2A and MM1C (Section 4.1.5; Fig. 7), illustrate three successive scenarios in the cave following the LGM sometime ~24–16 ka (Fig. 2; Table 1). The sorting and grading of sediment in mf 6a (Fig. 7A) is comparable to sedimentary crusts typically formed by rainfall in tropical regions experiencing varying aridity (Williams et al., 2018: 546–547). At TPL, this was more likely formed through $CaCO_3$-charged water droppings from the cave ceiling. The heavily compressed poorly sorted coarse sediment in mf 6b reflects that of a slaked crust, formed via the rapid wash in of damp sediments and their subsequent compression due to the trapped air in them (Bresson and Valentin, 1993), likely during the wet season. The vesicular-vughy and fused clayey aggregates in mf6c seen at the top of MM2A and MM1C (Fig. 7A and B) are distinctive of 'compaction crusts' resulting from 'aggregate deformation' under wet conditions (Bresson and Valentin, 1993: 748). In succession, these facies imply that ground conditions in TPL ~24–12 ka were often wet. Although crusting, and the ubiquitous Fe-oxide rich sediments (Vepraskas et al., 2018) suggest that the sediments were likely not as damp as conditions reconstructed for MIS 3 in TPL (Section 5.1.1–5.1.2). Intermittent dry conditions are evidenced by the more prominent voids in mf 6a and lower part of mf 6c (Fig. 7A and B), and some localised neoformation of sparites requiring more temperate conditions to form (White, 2007). This seasonal wet and dry conditions in TPL, is corroborated by the increased values of χ ~1.6 m (Fig. 10, Supplementary Table 2). Such conditions simultaneously reflect the regularity of monsoon rains and aridity in the region beginning the LGM ~20–11.5 ka and possibly earlier (Aggarwal et al., 2004; Marwick and Gagan, 2011) that would have promoted a temperate atmosphere in TPL at this time.

5.1.5. Unit 5–4, thin sections MM1B and MM1A: increased seasonality, marked periods of wet and dry cave conditions ~16–10 ka

The micromorphology of thin section MM1B and MM1A (Figs. 8 and 9) suggest increasingly wet ground conditions, punctuated by arid periods during the Late Pleistocene–Holocene transition ~16–12 ka and later. This is interpreted primarily from the six microfacies describing sediments from Unit 5–4 (Table 1). The compact finely bedded microstructure and intercalated features of mf 5a (Table 1; Section 4.1.6) suggest that low energy sedimentation deposited these sediments with intermittent input from coarse materials such as gravel-sized fragments of charcoal and bone (Fig. 8B). Such features have been observed at the Pinnacle Point archaeological cave site in South Africa (Karkanas and Goldberg, 2010). Research in this site interprets these features as accumulation zones and suggests that minor ponding contributed to the formation of this type facies. At TPL however, intercalating lenses in mf 5a formed by ponding of fine sediments is rather negligible when contrasted to coarse inclusions. The values of χ, OM and CC from 1.4 to 1.2 m below ground level (Supplementary Table 2; Fig. 10) corroborate this observation, with decreased χ likely suggesting a period of aridity accompanied by an increased input of both autogenic and allogenic sediments in the cave. These results reflect mf 5a as a relatively stable surface with significant accumulation derived primarily from dry colluviated coarse sediment. The moderate sorting of rip up clasts suspended in the Ca-rich feldspar clays of mf 5b (Fig. 8A–C) overlying mf 5a is interpreted as an alluvial deposit (Table 1) following similarities in structure to slackwater deposits recorded at Boila Rockshelter in Northwest Greece (Woodward et al., 2001). At TPL, the succession of mf 5a and 5b highlights a significant hydrological shift from moderately dry to wet ground conditions at the cave and likely of its environment in

general.

The succeeding overlying microfacies comprise those describing the base of Unit 4, likely deposited early in the Holocene (Table 1; Supplementary Table 1; Section 4.1.7). These microfacies are distinct to the rest of the microfacies observed throughout the studied sequence in that they possess distinctly well-developed primary structures (blocks, plates, channels) distinguished by moderate to poor structural accommodation (Fig. 9) suggesting that they have either been bioturbated (mf 4a; Fig. 2), crusted, and severely desiccated (mf 4b–d; Fig. 9E–G), although all these microfacies were primarily deposited via rather intense wet colluviation, noting their thickness and dense compaction. Combined with the interpretation of a hydrological shift between mf 5a and 5b, microfacies in Unit 4 indicate increased seasonality at TPL marked by distinct periods of wet and dry cave conditions. This interpretation is corroborated by the increased values of χ in sediments ~1.4–1.2 m in the sequence (Fig. 11; Table 1). Considering the micromorphological characteristics of microfacies from these units, the entrance to TPL may have significantly enlarged during the Late Pleistocene-Holocene transition. This would have permitted atmospheric conditions to strongly influence sedimentation and structural differentiation of the cave sediments despite the cover of forest canopy that is suggested to have surrounded it (Milano et al., 2018; McAllister-Hayward et al., 2024).

5.2. Taphonomic history of human fossils deposited from ~52 to 30 ka

Given the lack of intensive human activity at the site and the absence of definitive occupation of the cave, there begs the question of how the human fossils came to rest in the locations where they have been found. The taphonomic history of the fossils recovered from the upper 4 m of sediment in TPL is reconstructed using the inferred environmental conditions at the site from ~52 to 30 ka (Section 5.1.1–5.1.2). Although the environment in this part of the cave, where T3 is located, is frequently wet, the depositional processes interpreted from the microstratigraphic analyses and the types of sediment recorded do differ. These processes help us understand the deposition of the human fossils and their taphonomic history up to the point of discovery.

The depositional processes we reconstruct here only worked to redistribute the fossils to this low-lying part of the cave, explaining their discovery as disarticulated skeletal elements. For their deposition to occur in the region of T3, the fossils would have required either a more dynamic transportation process, or a much slower one with a longer period of transport. As such, it is likely that these fossils were present in this part of the cave from at least ~52–40 ka since they are well-preserved and do not exhibit signs of abrasion due to transport (Demeter et al., 2012, 2015).

5.2.1. Burial context of TPL2 and 5 (~52–40 ka): sheetflow on low bed angle

The human mandible (*TPL2*) and phalanx (*TPL5*) were excavated from 2.65 m below ground level from compact, dark reddish-brown silty clay with fine gravel and manganese oxide nodules deposited ~52–40 ka (Supplementary Table 1). The fine gravel stringers (Section 4.1.1; Fig. 3A) that underlie these sediments ~2.77 m suggest that aggradation through (horizontal) low energy sheetflow likely deposited these fossils into this part of the cave (Section 5.1.1). Sedimentological data from disaggregated samples ~2.8–2.6 m (Supplementary Table 1; Fig. 10) support this interpretation, showing that calcareous and organic materials were regularly being reworked into this part of the cave in decreasing order until they were later buried by the slumped deposits of clasts ~2.5 m, likely products of roof spalling (Section 5.1.2). The data also suggests that most of the sediments reworked in the cave were autogenic, and that much of the coarse debris had been deposited in the cave for some time. It is likely that these included the fossils *TPL2* and *5*.

5.2.2. Burial context of TPL1 (~48–30 ka): sloped sedimentation and slump action

The human skull (*TPL1*) was excavated at 2.36 m below ground level from reddish brown silty clays with manganese oxide nodules deposited ~48–30 ka (Supplementary Table 1). The cave conditions around this time were humid with the chamber grounds being mostly damp (Section 5.1.2). These conditions changed from wetter and temperate conditions earlier in MIS 3–52–40 ka (Section 5.1.1). Spalls and gravel clasts were recorded during field sampling ~2.34–2.50 m below ground level (Supplementary Table 1) and during microstratigraphic analysis as frequently occurring in sediments in mf 8b (Section 4.1.2; Fig. 4A). These are at the same level from which *TPL1* was found. It is likely that spalling or even a larger ceiling collapse coincided with these changes in the environment of the cave. Climatic changes have been recognised to result in geomorphic changes in cave systems (White, 1988; White, 2007). These include localised topographic shifts such as what we observe in thin sections from MM3 (Section 4.1.2) often caused by ceiling collapse and accompanying spalling. As observed across different environmental cave settings, such events can effectively remobilise surrounding sediment on newly formed slopes, where, depending on the scale of topographic disturbance and slope angle created, can be a few centimetres to metres thick or wide (Karkanas and Goldberg, 2010; Waters et al., 2021; Varis et al., 2022). At TPL, ~48–30 ka, our micromorphological observations suggest that slump and sloped deposition caused by significant cave attrition did not only include spalls and gravels, but sediments that have already been buried in the cave for some time (Fig. 4G–J), including the *TPL1* fossil.

5.3. Micro-traces of combustion: early human presence in Tam Pà Ling or natural fires

The micromorphology of TPL reveals micro-traces of combustion in the sediments such as charcoal (e.g., Fig. 3 C) and ash (e.g., Fig. 4 H) that can be related to specific depositional contexts inside the cave from ~52 to 10 ka (Table 1). These biproducts of combustion may represent human activity around the entrance of TPL or even in the cave during periods when ambient conditions were found to be temperate or mildly humid (Fig. 11). Alternatively, these traces of combustion may have come from small natural fires ignited during periods when regional climate was more arid and therefore conducive for such fire events to occur (e.g., during El Niño-like conditions). However, on the bases of the current evidence emanating from TPL and its surrounding environment, determining which is more likely of the two scenarios is difficult to ascertain.

Charcoal is produced by the incomplete combustion of a fuel, which is often wood or other plant materials, and low-temperature or dispersed burning for short periods of time (Scott, 2010; Mallol et al., 2017). In TPL, traces of charcoal are observed in mf 8a, 8c, 8e, 7, 6c, 5a, 5b and 4b (Table 1). Although they are uncommon in the sediment, these charcoal are often well-preserved as suggested by the articulated structure of plant fibres and vessels (e.g., Fig. 3C; 5G; 6B; 7J). Such preserved structures are indicative of minimal taphonomic modification (Scott, 2010), with research on the taphonomy of macroscopic charcoal (>125 μm) showing that these materials can preserve well when part of rapid sediment deposition, not transported from afar, and buried for a longer period of time (Théry-Parisot et al., 2010; Jha et al., 2021).

When burning occurs within a controlled area, for a longer period of time, or when temperatures exceed ~500 °C, calcination occurs and ash is produced (Canti and Brochier, 2017). Fully calcined ash is observed as micritic calcite, often exhibiting a rhomboidal structure in thin section. However, as it is of the same chemical composition as calcites in karstic environments, it is best to be cautious in interpreting micritic calcite in caves as wood or plant ash when these occur independently of charcoal, burnt sediment, or both. In TPL, these traces of combustion are microstratigraphically associated in mf 8a (Fig. 3D and E), mmf8c (Fig. 4H), mf 6C (Fig. 7J) and mf 5B (Fig. 8). Karkanas (2021) shows that ash from

hearths preserve more readily in redoximorphic environments, especially in caves, where the conditions allow the absorption and reprecipitation of mineral solutes within the porous spaces of ash to cement it in their primary context. His research suggests that when hearths are used several times, the biproducts of its combustion may be preserved even more. Hence, when these features are mechanically eroded, there is a good possibility that the ash, charcoal and even fragments of the oxidised substrate on which the hearth was lit is redeposited into different depositional environments in close context of each other such as we have seen in mf8a (Fig. 3D and E).

5.3.1. The probability of human activity at Tam Pà Ling

Together with the human fossils, the presence of ash and charcoal in most of the investigated microfacies hint that modern humans may have lit fires around the entrance or even inside TPL from at least ~52 ka to the end of the Pleistocene. Burning events during these periods, and the Holocene, are also implied by the magnetic susceptibility data, and its correlation with organic and carbonate values in the sediment (Section 4.2; Fig. 10). Combined, the data suggests that humans may have used TPL in the past for brief periods of time. In the Late Pleistocene, this was likely during periods when the ambient conditions in the cave were temperate or mildly humid ~52–40 ka and ~16–10 ka (Section 4.1.1; Fig. 3C–E; Section 4.1.5; Fig. 7D–F, I–J; Section 4.1.6; Fig. 8B–D–E, I), with the evidence of extensive occupation in the neighbouring Tam Hang rockshelter (Fig. 1B; Demeter et al., 2009; Patole-Edoumba, 2016) hinting at a greater possibility of more frequent human visits to the cave late in MIS 2 (and the Holocene) then earlier in MIS 3 when no clear occupation sites in the immediate landscape have so far been identified. However, if modern humans did engage in pyrotechnology at TPL during these periods then this did not occur in the areas of the cave where we have excavated so far as no hearth features have been recognised and, other than the fossils themselves, no convincing traces of human presence, such as trample zones or structured burning features have been discerned. Although the extensive scatter of massive rock fall throughout the cave (Fig. 1D) makes further exploration for these activity features difficult through traditional archaeological excavation, further micro-geoarchaeological prospection on the talus slopes, which have been demonstrated in other sites to potentially preserve palaeosurfaces and even archaeologically significant materials such as charcoal (Field and Banning, 1998; Berna et al., 2021; Brancaleoni et al., 2021), should elucidate this point.

5.3.2. Natural fires

Natural forest fires generally occur when climate is hot and dry. While the occurrence of forest fires is minimised in the C_3 vegetation dominated landscapes of SEA during glacials, when the region was found to be more humid, experienced less seasonality and received more rainfall (Wang et al., 1999), research has demonstrated the occurrence of forest fires in parts of SEA during dry periods from MIS 3–1 (Hamilton et al., 2019, 2020; Chen et al., 2024). Therefore, the occurrence of such fires cannot be discounted as the source of the microtrace evidence of combustion observed in TPL given the absence of intact hearth features from areas of the cave that have so far been excavated.

The microstratraphic evidence (Section 4.1) and plant wax biomarker data (McAllister-Hayward et al. (2024: 108471) that demonstrates variable moisture availability during MIS 3–2 in TPL and its surrounding landscape suggest that during periods within MIS 3 when moisture availability was low, there were 'breaks in the forest canopy, with potential increases in open patches of landscape. Yamoah et al. (2021) found that during mid MIS 3, when the *TPL1*, *2*, and *5* human fossils were deposited in T3, strong El Niño-like conditions prevailed over SEA leading to forest fires depositing concentrations of charcoal in Lake Pa Kho, northeastern Thailand. In TPL, similar scenarios may have occurred during this period and into MIS 2, when conditions around the region are noted to be more arid and the regional forest landscape was more open (Marwick and Gagan, 2011; Milano et al., 2018; McAllister-Hayward et al., 2024), which may have allowed patches of dry grass to burn and be deposited inside the cave (e.g., Fig. 4D).

Although present in most of the investigated microfacies, the biproducts of combustion in TPL are few (Table 1) and so do not likely relate to large scale, area specific fire events that would leave ample amounts of charcoal in the stratigraphy. Minor and confined fires are noted to only burn the (dry) forest understory since overstory burning results in massive wildfires and concentrations of combusted materials (Watts and Kobziar, 2013). In TPL, the exception would be the fine band of charcoal overlain by pale white fine sands that was noted ~0.75 m below ground level, which would have formed sometime during the mid-late Holocene (Supplementary Table 1). During this period, the modelled climate in the northwest of Laos shows that this region of mainland SEA experienced megadroughts (Griffiths et al., 2020), which would have been conducive for large-scale forest fires to occur. If so, then the fires would have deposited combusted materials widely in the sedimentary record of the region, possibly including the Holocene-dated sequence of sediments at TPL.

5.4. Variable preservation of materials within microfacies: implications for archaeological research in tropical cave sites

The detailed reconstruction of the depositional history at TPL has demonstrated that different processes delivered sediment from different areas of the cave, and, as we have shown (Section 5.1.1–5.1.5), these areas had unique depositional histories and thus circumstances and environments for the preservation—or not—of materials. Bone is notable in this instance. Bone in different states of preservation exist together, especially in microfacies associated with sediment deposited during MIS 3from ~52 to 30 ka (Sections 4.1.1–4.1.2, Figs. 3 and 4). As bone is an open system, the bioapatite contained in it, which holds important biomarkers such as DNA, can be easily leached into the sediment, often leaving only the mineralised/fossilised bone for morphological study. However, as we have demonstrated, finer fragments of bone ranging in the mm-sizes can still be preserved within the well-dated (and contextualised) stratigraphy. This is important as it has not been possible to extract aDNA from any of the TPL fossils so far. Thus, the 'excavation' and application of geoscience techniques at the micro level to aide in the sampling of these important biomarkers is therefore recommended (Morley et al., 2023; Aldeias and Stahlschmidt, 2024), especially on these tropical sediments (Morley, 2017). At this stage, the notion that organic materials useful for the study of the human past are poorly preserved or removed from tropical sedimentary environments is less tenable, especially since there have been great strides in demonstrating that aDNA (Massilani et al., 2022) and other biomarkers such as from plant waxes (Rabett et al., 2017; McAllister-Hayward et al., 2024) can be preserved and extracted from contexts and materials often thought to be of little use.

6. Conclusion

Our microstratigraphic approach to reconstruct the depositional history at TPL has proven effective in reconstructing the environments present in the cave from MIS3–1 (52–10ka). Although our reconstruction is restricted to the sedimentary sequence immediately north of where the mandible (*TPL2*), phalanx (*TPL5*) and skull (*TPL1*) were excavated, it has been representative of the sediments studied as these are laterally continuous for the most part in the large excavation area. Our analysis has determined low energy colluvial sedimentation and regular cave spalling as major components of the upper 4 m of the cave sequence. Conditions in this part of the cave were wet, but not inundated for long periods of time from 50 to 30 ka, shifting from being temperate from ~52–40 ka to humid ~48–30 ka. A short period of aridity is experienced in the cave during the LGM ~24 ka, with a return to wet and temperate cave conditions soon after, which is marked by distinct seasonality from ~16 ka through to the Holocene, when cave conditions

became predominantly dry.

The circumstances and conditions of the burial of *TPL2*, *5*, and *1*, which have all been excavated from sediment deposited during MIS 3 differ. We demonstrate that *TPL2* and 5 were deposited in this part of the cave via lateral (sheetflow) sedimentation during wet and temperate cave conditions, while *TPL1* was deposited downslope via slump action accompanying a shift in the interior topography of the cave during more humid conditions. However, all three would have been deposited in the chamber earlier than ~52–40 ka, before being further re-worked into the locations in which they were excavated.

By having identified plant ash, and well-preserved charcoal we present two possible scenarios for TPL. The first is that humans may have occasionally visited the cave, more so throughout MIS 3 and during the terminal Pleistocene ~16–10 ka than during the LGM (~24–12 ka). It is possible that TPL served as an occasional refuge for *Homo sapiens* passing through the area during the severely arid periods of MIS3 and towards the end of the Pleistocene ~12 ka and was not likely ever occupied or visited for long periods at a time. The second is that forest fires could have occurred during periods of severe aridity recorded in the region during MIS 3–1. These fires would have only been small and limited to open patches in the forest canopy prevalent throughout this period, and its biproducts only washed in during monsoons, when the more temperate conditions in TPL helped to preserve them.

By showing that materials may preserve differently within the same microstratigraphic units, we challenge the general assumption that preservation in tropical environments is always poor. This highlights the importance of conducting finer stratigraphic investigation of sites, especially at those where the consequence to our understanding of human evolution and dispersals are significant. Investigations such as these, when coupled with other techniques, can efficiently and effectively direct precise sampling for organic biomarkers—including aDNA—traditionally thought unlikely to preserve in the often hot and humid conditions of the tropics. This is especially true for tropical mainland SEA where climatic conditions have been found to be variable during the Late Pleistocene–Holocene (~52–10 ka), particularly at TPL.

Credit author statement

Conceptualisation, Investigation and Methodology: V.C.H. and M.W.M., Formal analysis and Visualisation: V.C.H., Validation: M.W.M., Writing — original draft: V.C.H., Writing — review and editing: M.W.M, A-M.B., P.D., K.E.W., R.J-B., J-L.P., C.Z., P.S., S.B., T.L., J-J.H., F.D.

Declaration of competing interest

The authors declare that they have no known competing financial interests or personal relationships that could have appeared to influence the work reported in this paper.

Data availability

Data will be made available on request.

Acknowledgements

The authors thank the Ministry of Information, Culture and Tourism of Laos, PDR for encouraging and supporting the research at TPL and the authorities of Xon district, Hua Pan Province and the villagers of Long Gua Pa for the support of the fieldwork there. The authors also thank the two reviewers for the useful comments and suggestions that helped improve the paper. V.C.H. thanks Flinders Archaeology Technical Officers Chantal Wight and Simon Hoad for facilitating with the work at the quarantine area of Flinders Microarchaeology Laboratory. M.W.M. and K.E.W. are supported by the Australian Research Council (ARC) through a Future Fellowship (FT180100309) and Discovery Project grant (DP170101597), respectively. Additional funding to support the fieldwork in Laos was provided by the following laboratories: UMR7206, MNHN through F.D.; Université de Paris through A.-M.B.; Université de Paris through P.D., and Department of Human Evolution, Max Planck Institute for Evolutionary Anthropology through J.-J. H., and the Sodipram Company and Porte-rêves Association, France. V.C.H. conducted this research through the support of a Flinders International Postgraduate Research Fellowship and ARC funding through M. W.M.

The authors pay tribute to Professors Yves Coppens and Thongsa Sayavongkhamdy who supported the work at TPL since 2003. Without their help the current research in the region would not have been possible. V.C.H. pays tribute to Professor Victor J. Paz who started him in archaeology.

Appendix A. Supplementary data

Supplementary data to this article can be found online at https://doi.org/10.1016/j.quascirev.2024.108982.

References

Aggarwal, P.K., Fröhlich, K., Kulkarni, K.M., Gourcy, L.L., 2004. Stable isotope evidence for moisture sources in the asian summer monsoon under present and past climate regimes. Geophys. Res. Lett. 31. https://doi.org/10.1029/2004GL019911.

Aldeias, V., Stahlschmidt, M.C., 2024. Sediment DNA can revolutionize archaeology—if it is used the right way. In: Proceedings of the National Academy of Sciences, vol. 121, e2317042121. https://doi.org/10.1073/pnas.2317042121.

Anderson, H.E., Morley, M.W., McAdams, C., Zaim, J., Rizal, Y., Aswan, Puspaningrum, M.R., Hascaryo, A.T., Price, G.J., Louys, J., 2024. The microstratigraphy and depositional environments of Lida Ajer and Ngalau Gupin, two fossil-bearing tropical limestone caves of west Sumatra. Sci. Rep. 14, 259. https://doi.org/10.1038/s41598-023-50975-8.

Bacon, A.-M., Bourgon, N., Welker, F., Cappellini, E., Fiorillo, D., Tombret, O., Thi Mai Huong, N., Anh Tuan, N., Sayavonkhamdy, T., Souksavatdy, V., Sichanthongtip, P., Antoine, P.-O., Duringer, P., Ponche, J.-L., Westaway, K., Joannes-Boyau, R., Boesch, Q., Suzzoni, E., Frangeul, S., Patole-Edoumba, E., Zachwieja, A., Shackelford, L., Demeter, F., Hublin, J.-J., Dufour, É., 2021. A multi-proxy approach to exploring Homo sapiens' arrival, environments and adaptations in Southeast Asia. Sci. Rep. 11, 21080. https://doi.org/10.1038/s41598-021-99931-4.

Beck, H.E., Zimmermann, N.E., McVicar, T.R., Vergopolan, N., Berg, A., Wood, E.F., 2018. Present and future Köppen-Geiger climate classification maps at 1-km resolution. Sci. Data 5, 180214. https://doi.org/10.1038/sdata.2018.214.

Benedetti, M.M., Haws, J.A., Bicho, N.F., Friedl, L., Ellwood, B.B., 2019. Late Pleistocene site formation and paleoclimate at Lapa do Picareiro, Portugal. Geoarchaeology 34, 698–726. https://doi.org/10.1002/gea.21735.

Berna, F., Boaretto, E., Wiebe, M.C., Goder-Goldberger, M., Abulafia, T., Lavi, R., Barzilai, O., Marder, O., Weiner, S., 2021. Site formation processes at Manot Cave, Israel: interplay between strata accumulation in the occupation area and the talus. J. Hum. Evol. 160, 102883. https://doi.org/10.1016/j.jhevol.2020.102883.

Bertran, P., 1993. Deformation-induced microstructures in soils affected by mass movements. Earth Surf. Process. Landforms 18, 645–660. https://doi.org/10.1002/esp.3290180707.

Bertran, P., Texier, J.-P., 1999. Facies and microfacies of slope deposits. Catena 35, 99–121. https://doi.org/10.1016/S0341-8162(98)00096-4.

Bourgon, N., Jaouen, K., Bacon, A.-M., Dufour, E., McCormack, J., Tran, N.H., Trost, M., Fiorillo, D., Dunn, T.E., Zanolli, C., Zachwieja, A., Duringer, P., Ponche, J.-L., Boesch, Q., Antoine, P.-O., Westaway, K.E., Joannes-Boyau, R., Suzzoni, E., Frangeul, S., Crozier, F., Aubaile, F., Patole-Edoumba, E., Luangkhoth, T., Souksavatdy, V., Boualaphane, S., Sayavonkhamdy, T., Sichanthongtip, P., Sihanam, D., Demeter, F., Shackelford, L.L., Hublin, J.-J., Tütken, T., 2021. Trophic ecology of a Late Pleistocene early modern human from tropical Southeast Asia inferred from zinc isotopes. J. Hum. Evol. 161, 103075. https://doi.org/10.1016/j.jhevol.2021.103075.

Bradák, B., Carrancho, Á., Herrejón Lagunilla, Á., Villalaín, J.J., Monnier, G.F., Tostevin, G., Mallol, C., Pajović, G., Baković, M., Borovinić, N., 2020. Magnetic fabric and archaeomagnetic analyses of anthropogenic ash horizons in a cave sediment succession (Crvena Stijena site, Montenegro). Geophys. J. Int. 224, 795–812. https://doi.org/10.1093/gji/ggaa461.

Brancaleoni, G., Shnaider, S., Osipova, E., Danukalova, G., Kurbanov, R., Deput, E., Alisher kyzy, S., Abdykanova, A., Krajcarz, M.T., 2021. Depositional history of a talus cone in an arid intermontane basin in Central Asia: an interdisciplinary study at the Late Pleistocene–Late Holocene Obishir-I site, Kyrgyzstan. Geoarchaeology 37, 350–373. https://doi.org/10.1002/gea.21892.

Brasseur, B., Sémah, F., Sémah, A.-M., Djubiantono, T., 2015. Pedo-sedimentary dynamics of the Sangiran dome hominid bearing layers (Early to Middle Pleistocene, central Java, Indonesia): a palaeopedological approach for reconstructing 'Pithecanthropus' (Javanese Homo erectus) palaeoenvironment. Quat. Int. 376, 84–100. https://doi.org/10.1016/j.quaint.2014.05.030.

Bresson, L.M., Valentin, C., 1993. Soil surface crust formation: contribution of micromorphology. In: Ringrose-Voase, A.J., Humphreys, G.S. (Eds.), Developments

in Soil Science. Elsevier, pp. 737–762. https://doi.org/10.1016/S0166-2481(08)70460-4.
Canti, M.G., 2003. Aspects of the chemical and microscopic characteristics of plant ashes found in archaeological soils. Catena 54, 339–361. https://doi.org/10.1016/S0341-8162(03)00127-9.
Canti, M.G., Brochier, J.É., 2017. Plant Ash, Archaeological Soil and Sediment Micromorphology 147–154. https://doi.org/10.1002/9781118941065.ch17.
Chabangborn, A., Brandefelt, J., Wohlfarth, B., 2014. Asian monsoon climate during the Last Glacial Maximum: palaeo-data–model comparisons. Boreas 43, 220–242. https://doi.org/10.1111/bor.12032.
Chen, Q., Huang, X., Tu, H., Shao, Q., Sun, X., Liu, Q., Wang, W., Lai, Z., Yang, X., 2024. Forces driving ecological degradation in southern China during the MIS3: natural or anthropogenic? Palaeogeogr. Palaeoclimatol. Palaeoecol. 640, 112088. https://doi.org/10.1016/j.palaeo.2024.112088.
Courty, M.-A., 2001. Microfacies analysis assisting archaeological stratigraphy. In: Goldberg, P., Holliday, V.T., Ferring, C.R. (Eds.), Earth Sciences and Archaeology. Springer US, Boston, MA, pp. 205–239. https://doi.org/10.1007/978-1-4615-1183-0_8.
Dearing, J.A., 1994. Environmental magnetic susceptibility: using the Bartington MS2 system. Chi Pub. https://gmw.com/wp-content/uploads/2019/03/JDearing-Handbook-OM0409.pdf.
Demeter, F., Bae, C.J., 2020. Dispersal barriers into Southeast Asia during the late pleistocene. Quat. Int. 563, 1–4. https://doi.org/10.1016/j.quaint.2020.09.035.
Demeter, F., Sayavongkhamdy, T., Pätole-Edoumba, E., Coupey, A.-S., Bacon, A.-M., Vos, J., Tougard, C., Bouasisengpaseuth, B., Sichanthongtip, P., Duringer, P., 2009. Tam Hang rockshelter: preliminary study of a prehistoric site in northern Laos. Asian Perspect. 48, 291–308. https://doi.org/10.1353/asi.2009.0000.
Demeter, F., Shackelford, L.L., Bacon, A.-M., Duringer, P., Westaway, K., Sayavongkhamdy, T., Braga, J., Sichanthongtip, P., Khamdalavong, P., Ponche, J.-L., Wang, H., Lundstrom, C., Patole-Edoumba, E., Karpoff, A.-M., 2012. Anatomically Modern Human in Southeast Asia (Laos) by 46 Ka, vol. 109. Proceedings of the National Academy of Sciences, 14375. https://doi.org/10.1073/pnas.1208104109.
Demeter, F., Shackelford, L., Westaway, K., Barnes, L., Duringer, P., Ponche, J.-L., Dumoncel, J., Sénégas, F., Sayavongkhamdy, T., Zhao, J.-X., Sichanthongtip, P., Patole-Edoumba, E., Dunn, T., Zachwieja, A., Coppens, Y., Willerslev, E., Bacon, A.-M., 2017. Early modern humans from Tam Pà ling, Laos: fossil review and perspectives. Curr. Anthropol. 58, S527–S538. https://doi.org/10.1086/694192.
Demeter, F., Shackelford, L., Westaway, K., Duringer, P., Bacon, A.-M., Ponche, J.-L., Wu, X., Sayavongkhamdy, T., Zhao, J.-X., Barnes, L., Boyon, M., Sichanthongtip, P., Sénégas, F., Karpoff, A.-M., Patole-Edoumba, E., Coppens, Y., Braga, J., 2015. Early modern humans and morphological variation in Southeast Asia: fossil evidence from Tam Pa ling, Laos. PLoS One 10, e0121193. https://doi.org/10.1371/journal.pone.0121193.
Demeter, F., Zanolli, C., Westaway, K.E., Joannes-Boyau, R., Duringer, P., Morley, M.W., Welker, F., Rüther, P.L., Skinner, M.M., McColl, H., 2022. A Middle pleistocene denisovan molar from the annamite chain of northern Laos. Nat. Commun. 13, 2557. https://doi.org/10.1038/s41467-022-29923-z.
Dennell, R., 2017. Human colonization of Asia in the late pleistocene: the history of an invasive species. Curr. Anthropol. 58, S383–S396. https://doi.org/10.1086/694174.
Dinckal, A., Fisher, E.C., Herries, A.I.R., Marean, C.W., 2022. Mapping magnetism: geophysical modelling of stratigraphic features by using in situ magnetic susceptibility measurements at Pinnacle Point 5-6 North, South Africa. Geoarchaeology 37, 840–857. https://doi.org/10.1002/gea.21924.
Duringer, P., Bacon, A.-M., Sayavongkhamdy, T., Nguyen, T.K.T., 2012. Karst development, breccias history, and mammalian assemblages in Southeast Asia: a brief review. Comptes Rendus Palevol 11, 133–157. https://doi.org/10.1016/j.crpv.2011.07.003.
Evans, M., Heller, F., 2003. Environmental Magnetism: Principles and Applications of Enviromagnetics. Elsevier. eBook. ISBN: 9780080505787.
Ferro-Vázquez, C., Mallol, C., Aldeias, V., 2022. Simply red? A systematic colour-based method for identifying archaeological fires. Geoarchaeology 37, 284–303. https://doi.org/10.1002/gea.21886.
Field, J., Banning, E.B., 1998. Hillslope processes and archaeology in wadi ziqlab, Jordan. Geoarchaeology 13, 595–616. https://doi.org/10.1002/(SICI)1520-6548(199808)13:6<595::AID-GEA4>3.0.CO;2-U.
Freidline, S.E., Westaway, K.E., Joannes-Boyau, R., Duringer, P., Ponche, J.-L., Morley, M.W., Hernandez, V.C., McAllister-Hayward, M.S., McColl, H., Zanolli, C., 2023. Early presence of Homo sapiens in Southeast Asia by 86–68 kyr at Tam Pà ling, northern Laos. Nat. Commun. 14, 3193. https://doi.org/10.1038/s41467-023-38715-y.
Friesem, D.E., Shahack-Gross, R., Weinstein-Evron, M., Teutsch, N., Weissbrod, L., Shimelmitz, R., 2021. High-resolution study of Middle Palaeolithic deposits and formation processes at Tabun Cave, Israel: guano-rich cave deposits and detailed stratigraphic appreciation of Layer C. Quat. Sci. Rev. 274, 107203. https://doi.org/10.1016/j.quascirev.2021.107203.
Fromaget, J., Saurin, E., 1936. Note préliminaire sur les formations Cénozoiques et plus récentes de la chaîne Annamitique septentrionale et du Haut-Laos (stratigraphie, préhistoire, anthropologie). Bulletin du Service Géologique de l'Indochine 22, 1–48.
Goldberg, P., 2001. Some micromorphological aspects of prehistoric cave deposits. Cahiers d'Archéologie du CELAT 10, 161–175. d1wqtxts1xzle7.cloudfront.net/32012637/Goldberg.
Goldberg, P., Aldeias, V., 2018. Why does (archaeological) micromorphology have such little traction in (geo)archaeology? Archaeological and Anthropological Sciences 10, 269–278. https://doi.org/10.1007/s12520-016-0353-9.
Griffiths, M.L., Johnson, K.R., Pausata, F.S.R., White, J.C., Henderson, G.M., Wood, C.T., Yang, H., Ersek, V., Conrad, C., Sekhon, N., 2020. End of green sahara amplified mid- to late Holocene megadroughts in mainland Southeast Asia. Nat. Commun. 11, 4204. https://doi.org/10.1038/s41467-020-17927-6.
Hamilton, R., Penny, D., Hall, T.L., 2020. Forest, fire & monsoon: investigating the long-term threshold dynamics of south-east Asia's seasonally dry tropical forests. Quat. Sci. Rev. 238, 106334. https://doi.org/10.1016/j.quascirev.2020.106334.
Hamilton, R., Stevenson, J., Li, B., Bijaksana, S., 2019. A 16,000-year record of climate, vegetation and fire from Wallacean lowland tropical forests. Quat. Sci. Rev. 224, 105929. https://doi.org/10.1016/j.quascirev.2019.105929.
Heiri, O., Lotter, A.F., Lemcke, G., 2001. Loss on ignition as a method for estimating organic and carbonate content in sediments: reproducibility and comparability of results. J. Paleolimnol. 25, 101–110. https://doi.org/10.1023/A:1008119611481.
Howard, J.L., Amos, D.F., Daniels, W.L., 1996. Micromorphology and dissolution of quartz sand in some exceptionally ancient soils. Sediment. Geol. 105, 51–62. https://doi.org/10.1016/0037-0738(95)00133-6.
Hublin, J.-J., 2021. How old are the oldest Homo sapiens in Far East Asia? Proc. Natl. Acad. Sci. USA 118, e2101173118. https://doi.org/10.1073/pnas.2101173118.
Hunt, C.O., Gilbertson, D.D., Rushworth, G., 2007. Modern humans in Sarawak, Malaysian Borneo, during oxygen isotope stage 3: palaeoenvironmental evidence from the Great Cave of Niah. J. Archaeol. Sci. 34, 1953–1969. https://doi.org/10.1016/j.jas.2007.02.023.
Jha, D.K., Samrat, R., Sanyal, P., 2021. The first evidence of controlled use of fire by prehistoric humans during the Middle Paleolithic phase from the Indian subcontinent. Palaeogeogr. Palaeoclimatol. Palaeoecol. 562, 110151. https://doi.org/10.1016/j.palaeo.2020.110151.
Karkanas, P., 2019. Microscopic deformation structures in archaeological contexts. Geoarchaeology 34, 15–29. https://doi.org/10.1002/gea.21709.
Karkanas, P., 2021. All about wood ash: long term fire experiments reveal unknown aspects of the formation and preservation of ash with critical implications on the emergence and use of fire in the past. J. Archaeol. Sci. 135, 105476. https://doi.org/10.1016/j.jas.2021.105476.
Karkanas, P., Goldberg, P., 2010. Site formation processes at Pinnacle point cave 13B (Mossel Bay, Western Cape province, South Africa): resolving stratigraphic and depositional complexities with micromorphology. J. Hum. Evol. 59, 256–273. https://doi.org/10.1016/j.jhevol.2010.07.001.
Kehl, M., Eckmeier, E., Franz, S., Lehmkuhl, F., Soler, J., Soler, N., Reicherter, K., Weniger, G.-C., 2014. Sediment sequence and site formation processes at the Arbreda Cave, NE Iberian Peninsula, and implications on human occupation and climate change during the Last Glacial. Clim. Past 10, 1673–1692. https://doi.org/10.5194/cp-10-1673-2014.
Lee, S.-H., Hudock, A., 2021. Human evolution in Asia: Taking stock and looking forward. Annu. Rev. Anthropol. 50, 145–166. https://doi.org/10.1146/annurev-anthro-101819-110230.
Lewis, H., 2007. Preliminary soil micromorphology studies of landscape and occupation history at Tabon Cave, Palawan, Philippines. Geoarchaeol. 22, 685–708. https://doi.org/10.1002/gea.20182.
Liu, W., Martinón-Torres, M., Cai, Y.-j., Xing, S., Tong, H.-w., Pei, S.-w., Sier, M.J., Wu, X.-h., Edwards, R.L., Cheng, H., Li, Y.-y., Yang, X.-x., Castro, J.M.B.d., Wu, X.-J., 2015. The earliest unequivocally modern human in southern China. Nature 526, 696–699. https://doi.org/10.1038/nature15696.
Louys, J., Kealy, S., O'Connor, S., Price, G.J., Hawkins, S., Aplin, K., Rizal, Y., Zaim, J., Tanudirjo, D.A., Santoso, W.D., 2017. Differential preservation of vertebrates in Southeast Asian caves. Int. J. Speleol. 46, 6. https://doi.org/10.5038/1827-806X.46.3.2131.
Lowe, K.M., Shulmeister, J., Feinberg, J.M., Manne, T., Wallis, L.A., Welsh, K., 2016. Using soil magnetic properties to determine the onset of pleistocene human settlement at gledswood shelter 1, northern Australia. Geoarchaeology 31, 211–228. https://doi.org/10.1002/gea.21544.
MacIntyre, I.G., Reid, R.P., 2003. Micritization. In: Middleton, G.V., Church, M.J., Coniglio, M., Hardie, L.A., Longstaffe, F.J. (Eds.), Encyclopedia of Sediments and Sedimentary Rocks. Springer, Netherlands, Dordrecht, pp. 436–438. https://doi.org/10.1007/978-1-4020-3609-5_136.
Macphail, R.I., Goldberg, P., 2017. Applied Soils and Micromorphology in Archaeology. Cambridge University Press, Cambridge. https://doi.org/10.1017/9780511895562.
Maher, B.A., 1998. Magnetic properties of modern soils and Quaternary loessic paleosols: paleoclimatic implications. Palaeogeogr. Palaeoclimatol. Palaeoecol. 137, 25–54. https://doi.org/10.1016/S0031-0182(97)00103-X.
Mallol, C., Mentzer, S.M., Miller, C.E., 2017. Combustion features. Archaeological Soil and Sediment Micromorphology, pp. 299–330. https://doi.org/10.1002/9781118941065.ch31.
Martinsen, O.J., 1978. Slide and Slump Structures, Sedimentology. Springer, Berlin Heidelberg, Berlin, Heidelberg, pp. 1104–1107. https://doi.org/10.1007/3-540-31079-7_213.
Marwick, B., Gagan, M.K., 2011. Late Pleistocene monsoon variability in northwest Thailand: an oxygen isotope sequence from the bivalve Margaritanopsis laosensis excavated in Mae Hong Son province. Quat. Sci. Rev. 30, 3088–3098. https://doi.org/10.1016/j.quascirev.2011.07.007.
Massilani, D., Morley, M.W., Mentzer, S.M., Aldeias, V., Vernot, B., Miller, C., Stahlschmidt, M., Kozlikin, M.B., Shunkov, M.V., Derevianko, A.P., Conard, N.J., Wurz, S., Henshilwood, C.S., Vasquez, J., Essel, E., Nagel, S., Richter, J., Nickel, B., Roberts, R.G., Pääbo, S., Slon, V., Goldberg, P., Meyer, M., 2022. Microstratigraphic preservation of ancient faunal and hominin DNA in Pleistocene cave sediments. Proc. Natl. Acad. Sci. USA 119, e2113666118. https://doi.org/10.1073/pnas.2113666118.
Matsumura, H., Hung, H.-c., Higham, C., Zhang, C., Yamagata, M., Nguyen, L.C., Li, Z., Fan, X.-c., Simanjuntak, T., Oktaviana, A.A., He, J.-n., Chen, C.-y., Pan, C.-k., He, G., Sun, G.-p., Huang, W.-j., Li, X.-w., Wei, X.-t., Domett, K., Halcrow, S., Nguyen, K.D.,

Trinh, H.H., Bui, C.H., Nguyen, K.T.K., Reinecke, A., 2019. Craniometrics reveal "two layers" of prehistoric human dispersal in eastern eurasia. Scientific reports 9, 1451.Demeter, F., Bae, C.J., 2020. Dispersal barriers into Southeast Asia during the late pleistocene. Quat. Int. 563, 1–4. https://doi.org/10.1038/s41598-018-35426-z.

McAdams, C., Morley, M.W., Fu, X., Kandyba, A.V., Derevianko, A.P., Nguyen, D.T., Doi, N.G., Roberts, R.G., 2020. The Pleistocene geoarchaeology and geochronology of Con Moong Cave, North Vietnam: site formation processes and hominin activity in the humid tropics. Geoarchaeology 35, 72–97. https://doi.org/10.1002/gea.21758.

McAdams, C., Morley, M.W., Roberts, R.G., 2021. The acid test: an experimental microarchaeological study of guano-driven diagenesis in tropical cave sediments. J. Archaeol. Sci.: Reports 37, 102947. https://doi.org/10.1016/j.jasrep.2021.102947.

McAllister, M.S., Morley, M.W., Tyler, J.J., McInerney, F.A., Blyth, A.J., 2022. Investigating the palaeoenvironmental context of Late Pleistocene human dispersals into Southeast Asia: a review of stable isotope applications. Archaeological and Anthropological Sciences 14, 86. https://doi.org/10.1007/s12520-022-01540-3.

McAllister-Hayward, M.S., Blyth, A.J., McInerney, F.A., Holman, A.I., Grice, K., Tyler, J. J., Westaway, K.W., Joannes-Boyau, R., Boualaphane, S., Bourgon, N., Dunn, T.E., Frangeul, S., Luangkhoth, T., Ponche, J.L., Sichanthongtip, P., Souksavatdy, V., Suzzoni, E., Zachwieja, A., Zanolli, C., Bacon, A.M., Duringer, P., Hublin, J.J., Shackelford, L., Demeter, F., Morley, M.W., 2024. Reconstructing the environmental conditions experienced by early modern humans at Tam Pà Ling (northeast Laos) using higher plant wax biomarkers. Quat. Sci. Rev. 325, 108471. https://doi.org/10.1016/j.quascirev.2023.108471.

Mentzer, S.M., 2014. Microarchaeological approaches to the identification and interpretation of combustion features in prehistoric archaeological sites. J. Archaeol. Method Theor 21, 616–668. https://doi.org/10.1007/s10816-012-9163-2.

Mijares, A.S., 2017. Understanding the callao cave depositional history. Terra Aust. 45, 125. https://doi.org/10.22459/TA45.03.2017.07.

Milano, S., et al., 2018. Environmental conditions framing the first evidence of modern humans at Tam Pà Ling, Laos: a stable isotope record from terrestrial gastropod carbonates. Palaeogeogr. Palaeoclimatol. Palaeoecol. 511, 352–363. https://doi.org/10.1016/j.palaeo.2018.08.020.

Morley, M.W., 2017. The geoarchaeology of hominin dispersals to and from tropical Southeast Asia: a review and prognosis. J. Archaeol. Sci. 77, 78–93. https://doi.org/10.1016/j.jas.2016.07.009.

Morley, M.W., Goldberg, P., 2017. Geoarchaeological research in the humid tropics: a global perspective. J. Archaeol. Sci. 77, 1–9. https://doi.org/10.1016/j.jas.2016.11.002.

Morley, M.W., Goldberg, P., Sutikna, T., Tocheri, M.W., Prinsloo, L.C., Jatmiko, Saptomo, E.W., Wasisto, S., Roberts, R.G., 2017. Initial micromorphological results from Liang Bua, Flores (Indonesia): site formation processes and hominin activities at the type locality of Homo floresiensis. J. Archaeol. Sci. 77, 125–142. https://doi.org/10.1016/j.jas.2016.06.004.

Morley, M.W., Moffat, I., Kotarba-Morley, A.M., Hernandez, V.C., Zerboni, A., Herries, A. I.R., Joannes-Boyau, R., Westaway, K., 2023. Why the geosciences are becoming increasingly vital to the interpretation of the human evolutionary record. Nature Ecology & Evolution 7, 1971–1977. https://doi.org/10.1038/s41559-023-02215-5.

Mücher, H., van Steijn, H., Kwaad, F., 2018. Chapter 2 - colluvial and mass wasting deposits. In: Stoops, G., Marcelino, V., Mees, F. (Eds.), Interpretation of Micromorphological Features of Soils and Regoliths, second ed. Elsevier, pp. 21–36. https://doi.org/10.1016/B978-0-444-63522-8.00002-4.

Nguyen-Le, D., Matsumoto, J., Ngo-Duc, T., 2015. Onset of the rainy seasons in the eastern indochina peninsula. J. Clim. 28, 5645–5666. https://doi.org/10.1175/JCLI-D-14-00373.1.

O'Connor, S., Barham, A., Spriggs, M., Veth, P., Aplin, K., St Pierre, E., 2010. Cave archaeology and sampling issues in the tropics: a case study from lene hara cave, a 42,000 Year old occupation site in east timor, island Southeast Asia. Aust. Archaeol. 71, 29–40. https://doi.org/10.1080/03122417.2010.11689382.

Patole-Edoumba, E., Duringer, P., Richardin, P., Shackelford, L., Bacon, A.-M., Sayavongkhamdy, T., Ponche, J.-L., Demeter, F., 2015. Evolution of the hoabinhian techno-complex of Tam Hang rock shelter in northeastern Laos. Archaeol. Discov. 3, 140. https://doi.org/10.4236/ad.2015.34013.

Piló, L.B., Auler, A.S., Neves, W.A., Wang, X., Cheng, H., Edwards, R.L., 2005. Geochronology, sediment provenance, and fossil emplacement at Sumidouro Cave, a classic late Pleistocene/early Holocene paleoanthropological site in eastern Brazil. Geoarchaeology: Int. J. 20, 751–764. https://doi.org/10.1002/gea.20081.

Rabett, R., Ludgate, N., Stimpson, C., Hill, E., Hunt, C., Ceron, J., Farr, L., Morley, M., Reynolds, T., Zukswert, H., Simpson, D., Nyiri, B., Verhoeven, M., Appleby, J., Meneely, J., Phan, L., Dong, N.N., Lloyd-Smith, L., Hawkes, J., Blyth, A., Tản, N.C., 2017. Tropical limestone forest resilience and late Pleistocene foraging during MIS-2 in the Tràng an massif, Vietnam. Quat. Int. 448, 62–81. https://doi.org/10.1016/j.quaint.2016.06.010.

Saminpanya, S., Denkitkul, N., 2020. Micromorphology, mineralogy, and geochemistry of sediments at the tham lod rock shelter archaeological site in Mae Hong Son, Thailand: suggestions of a late pleistocene climate. J. Cave Karst Stud. 51. https://doi.org/10.4311/2019ES0111.

Saurin, E., 1969. Les Recherches Préhistoriques au Cambodge, Laos, et Viet Nam (1877-1966). Asian Perspect. 12, 27–41 jstor.org/stable/42929061.

Sawafuji, R., Tsutaya, T., Takahata, N., Pedersen, M.W., Ishida, H., 2024. East and Southeast Asian hominin dispersal and evolution: a review. Quat. Sci. Rev. 333, 108669. https://doi.org/10.1016/j.quascirev.2024.108669.

Scerri, E.M., Roberts, P., Yoshi Maezumi, S., Malhi, Y., 2022. Tropical Forests in the Deep Human Past. The Royal Society, 20200500. https://doi.org/10.1098/rstb.2020.0500.

Scott, A.C., 2010. Charcoal recognition, taphonomy and uses in palaeoenvironmental analysis. Palaeogeogr. Palaeoclimatol. Palaeoecol. 291, 11–39. https://doi.org/10.1016/j.palaeo.2009.12.012.

Shackelford, L., Demeter, F., Westaway, K., Duringer, P., Ponche, J.-L., Sayavongkhamdy, T., Zhao, J.-X., Barnes, L., Boyon, M., Sichanthongtip, P., Sénégas, F., Patole-Edoumba, E., Coppens, Y., Dumoncel, J., Bacon, A.-M., 2018. Additional evidence for early modern human morphological diversity in Southeast Asia at Tam Pa Ling, Laos. Quat. Int. 466, 93–106. https://doi.org/10.1016/j.quaint.2016.12.002.

Shipton, C., Morley, M.W., Kealy, S., Norman, K., Boulanger, C., Hawkins, S., Litster, M., Withnell, C., O'Connor, S., 2024. Abrupt onset of intensive human occupation 44,000 years ago on the threshold of Sahul. Nat. Commun. 15, 4193. https://doi.org/10.1038/s41467-024-48395-x.

Skaberne, D., Turk, I., Turk, J., 2015a. The Pleistocene clastic sediments in the Divje babe I cave, Slovenia. Palaeoclimate (part 1). Palaeogeogr. Palaeoclimatol. Palaeoecol. 438, 395–407. https://doi.org/10.1016/j.palaeo.2015.07.033.

Skaberne, D., Turk, I., Turk, J., 2015b. The Pleistocene clastic sediments in the Divje babe I cave, Slovenia. Geochemical characterisation and provenance (Part 2). Palaeogeogr. Palaeoclimatol. Palaeoecol. 438, 379–394. https://doi.org/10.1016/j.palaeo.2015.07.032.

Sleep, N.H., Hessler, A.M., 2006. Weathering of quartz as an Archean climatic indicator. Earth Planet Sci. Lett. 241, 594–602. https://doi.org/10.1016/j.epsl.2005.11.020.

Smith, H.E., Morley, M.W., Louys, J., 2020. Taphonomic analyses of cave breccia in Southeast Asia: a review and future directions. Open Quat. 6, 1–22. https://doi.org/10.5334/oq.75.

Stephens, M., Rose, J., Gilbertson, D., Canti, M., 2005. The micromorphology of cave sediments in the humid tropics: niah Cave, Sarawak. Asian Perspect. 44 (1), 42–55. www.jstor.org/stable/42928634.

Stephens, M., Hunt, C., Rose, J., Canti, M., Gilbertson, D., McLaren, S., Grattan, J., Rushworth, G., 2016. The sedimentology of the West Mouth lithofacies. In: Barker, G., Farr, L. (Eds.), Archaeological Investigations in the Niah Caves, Sarawak. University of Cambridge, pp. 81–104 (Chapter 5). Volume 2. McDonald Research Institute.

Stephens, M., Rose, J., Gilbertson, D., 2017. Post-depositional alteration of humid tropical cave sediments: micromorphological research in the great cave of niah, sarawak, borneo. J. Archaeol. Sci. 77, 109–124. https://doi.org/10.1016/j.jas.2016.01.015.

Stoops, G., 1978. Some considerations on quantitative soil micromorphology, Micromorfologia de suelos. Proc. 5th Intern. Working Meeting Soil Microm. Granada, pp. 1367–1384.

Stoops, G., 2018. Micromorphology as a tool in soil and regolith studies. Interpretation of Micromorphological Features of Soils and Regoliths. Elsevier, pp. 1–19. https://doi.org/10.1016/B978-0-444-53156-8.00001-5.

Stoops, G., 2021. Guidelines for Analysis and Description of Soil and Regolith Thin Sections. John Wiley & Sons. https://doi.org/10.1002/9780891189763.fmatter.

Théry-Parisot, I., Chabal, L., Chrzavzez, J., 2010. Anthracology and taphonomy, from wood gathering to charcoal analysis. A review of the taphonomic processes modifying charcoal assemblages, in archaeological contexts. Palaeogeogr. Palaeoclimatol. Palaeoecol. 291, 142–153. https://doi.org/10.1016/j.palaeo.2009.09.016.

Tite, M.S., Mullins, C., 1971. Enhancement of the magnetic susceptibility of soils on archaeological sites. Archaeometry 13, 209–219. https://doi.org/10.1111/j.1475-4754.1971.tb00043.x.

Tsatskin, A., Gendler, T.S., 2016. Identification of "red ochre" in soil at Kfar HaHoresh Neolithic site, Israel: magnetic measurements coupled with materials characterization. J. Archaeol. Sci.: Reports 6, 284–292. https://doi.org/10.1016/j.jasrep.2016.02.027.

Van Den Berg, G.A., Loch, J.P.G., 2000. Decalcification of soils subject to periodic waterlogging. Eur. J. Soil Sci. 51, 27–33. https://doi.org/10.1046/j.1365-2389.2000.00279.x.

Varis, A., Miller, C.E., Cuthbertson, P., Namen, A., Taimagambetov, Z., Iovita, R., 2022. The effect of formation processes on the frequency of palaeolithic cave sites in semiarid zones: insights from Kazakhstan. Geoarchaeology 37, 594–616. https://doi.org/10.1002/gea.21909.

Vepraskas, M.J., Lindbo, D.L., Stolt, M.H., 2018. Chapter 15 - redoximorphic features. In: Stoops, G., Marcelino, V., Mees, F. (Eds.), Interpretation of Micromorphological Features of Soils and Regoliths, second ed. Elsevier, pp. 425–445. https://doi.org/10.1016/B978-0-444-63522-8.00015-2.

Wang, L., Sarnthein, M., Erlenkeuser, H., Grimalt, J., Grootes, P., Heilig, S., Ivanova, E., Kienast, M., Pelejero, C., Pflaumann, U., 1999. East asian monsoon climate during the late pleistocene: high-resolution sediment records from the South China sea. Mar. Geol. 156, 245–284. https://doi.org/10.1016/S0025-3227(98)00182-0.

Waters, M.R., Keene, J.L., Prewitt, E.R., Everett, M.E., Laughlin, T., Stafford, T.W., 2021. Late Quaternary geology, archaeology, and geoarchaeology of Hall's Cave, Texas. Quat. Sci. Rev. 274, 107276. https://doi.org/10.1016/j.quascirev.2021.107276.

Watts, A.C., Kobziar, L.N., 2013. Smoldering combustion and ground fires: ecological effects and multi-scale significance. Fire Ecology 9, 124–132. https://doi.org/10.4996/fireecology.0901124.

Weiner, S., 2010. Microarchaeology: beyond the Visible Archaeological Record. Cambridge University Press, Cambridge. https://doi.org/10.1017/CBO9780511811210.

Westaway, K.E., Louys, J., Awe, R.D., Morwood, M.J., Price, G.J., Zhao, J.x., Aubert, M., Joannes-Boyau, R., Smith, T.M., Skinner, M.M., Compton, T., Bailey, R.M., van den Bergh, G.D., de Vos, J., Pike, A.W.G., Stringer, C., Saptomo, E.W., Rizal, Y., Zaim, J., Santoso, W.D., Trihascaryo, A., Kinsley, L., Sulistyanto, B., 2017. An early modern

human presence in Sumatra 73,000–63,000 years ago. Nature 548, 322–325. https://doi.org/10.1038/nature23452.

White, W., 1988. Geomorphology and Hydrology of Karst Terrain. Oxford University Press, New York, p. 464p. ISBN: 9780195044447.

White, W., 2007. Cave sediments and paleoclimate. J. Cave Karst Stud. 69. https://caves.org/wp-content/uploads/Publications/JCKS/v69/cave-69-01-76.pdf.

Williams, A.J., Pagliai, M., Stoops, G., 2018. Chapter 19 - physical and biological surface crusts and seals. In: Stoops, G., Marcelino, V., Mees, F. (Eds.), Interpretation of Micromorphological Features of Soils and Regoliths, second ed. Elsevier, pp. 539–574. https://doi.org/10.1016/B978-0-444-63522-8.00019-X.

Woods, W.I., 2003. Development of Anthrosol Research, Amazonian Dark Earths: Origin Properties Management. Springer, pp. 3–14. https://doi.org/10.1007/1-4020-2597-1_1.

Woodward, J.C., Hamlin, R.H.B., Macklin, M.G., Karkanas, P., Kotjabopoulou, E., 2001. Quantitative sourcing of slackwater deposits at Boila rockshelter: a record of lateglacial flooding and Paleolithic settlement in the Pindus Mountains, Northwest Greece. Geoarchaeology 16, 501–536. https://doi.org/10.1002/gea.1003.

Wu, C.-H., Hsu, H.-H., 2016. Role of the indochina peninsula narrow mountains in modulating the East asian-Western north pacific summer monsoon. J. Clim. 29. https://doi.org/10.1175/JCLI-D-15-0594.1.

Yamoah, K.A., Chabangborn, A., Chawchai, S., Fritz, S., Löwemark, L., Kaboth-Bahr, S., Reimer, P.J., Smittenberg, R.H., Wohlfarth, B., 2021. A muted El Niño-like condition during late MIS 3. Quat. Sci. Rev. 254, 106782. https://doi.org/10.1016/j.quascirev.2020.106782.

Yao, Y., Liao, W., Bae, C.J., Sun, X., Feng, Y., Tian, C., Li, J., Wei, S., Wang, W., 2020. New discovery of Late Pleistocene modern human teeth from Chongzuo, Guangxi, southern China. Quat. Int. 563, 5–12. https://doi.org/10.1016/j.quaint.2020.02.002.

Zamanian, K., Pustovoytov, K., Kuzyakov, Y., 2016. Pedogenic carbonates: forms and formation processes. Earth Sci. Rev. 157, 1–17. https://doi.org/10.1016/j.earscirev.2016.03.003.